



A Geometric Approach to Phase Response Curves and Its Numerical Computation Through the Parameterization Method

Alberto Pérez-Cervera^{1,2} · Tere M-Seara^{1,2} · Gemma Huguet^{1,2}

Received: 19 September 2018 / Accepted: 24 June 2019 / Published online: 13 July 2019
© Springer Science+Business Media, LLC, part of Springer Nature 2019

Abstract

The phase response curve (PRC) is a tool used in neuroscience that measures the phase shift experienced by an oscillator due to a perturbation applied at different phases of the limit cycle. In this paper, we present a new approach to PRCs based on the parameterization method. The underlying idea relies on the construction of a periodic system whose corresponding stroboscopic map has an invariant curve. We demonstrate the relationship between the internal dynamics of this invariant curve and the PRC, which yields a method to numerically compute the PRCs. Moreover, we link the existence properties of this invariant curve as the amplitude of the perturbation is increased with changes in the PRC waveform and with the geometry of isochrons. The invariant curve and its dynamics will be computed by means of the parameterization method consisting of solving an invariance equation. We show that the method to compute the PRC can be extended beyond the breakdown of the curve by means of introducing a modified invariance equation. The method also computes the amplitude response functions (ARCs) which provide information on the displacement away from the oscillator due to the effects of the perturbation. Finally, we apply the method to several classical models in neuroscience to illustrate how the results herein extend the framework of computation and interpretation of the PRC and ARC for perturbations of large amplitude and not necessarily pulsatile.

Keywords Phase response curves · Isochrons · Phase equation · Parameterization method · NHIM · Synchronization

Communicated by Dr. Paul Newton.

✉ Alberto Pérez-Cervera
alberto.perez@upc.edu

¹ Departament de Matemàtiques, Universitat Politècnica de Catalunya, Avda. Diagonal 647, 08028 Barcelona, Spain

² BGSMath, Barcelona, Spain

Mathematics Subject Classification 37D10 · 92B25 · 65P99 · 37N30

1 Introduction

Oscillations are ubiquitous in the brain (Buzsaki 2006). From cellular to population level, there exist numerous recordings showing periodic activity. Mathematically, oscillations correspond to attracting limit cycles in the phase space whose dynamics can be described by a phase variable. Under generic conditions, the phase can be extended to a neighbourhood of the limit cycle via the concepts of asymptotic phase and isochrons (Guckenheimer 1975; Winfree 1974). Isochrons are the sets of points in the basin of attraction of a limit cycle whose orbits approach asymptotically the orbit of a given point on the limit cycle. We associate with these points the same phase as the base point on the limit cycle. The regions outside the basin of attraction are called phaseless sets (Guckenheimer 1975).

When the oscillator is perturbed with a transient external stimulus, the trajectory of each point is displaced away from the limit cycle and set to the isochron of a different point, thus causing a change in the phase of the oscillation. Phase displacements due to perturbations of the oscillator that act at different phases of the limit cycle are described by the so-called phase response curves (PRCs) (Ermentrout and Terman 2010; Schultheiss et al. 2011). PRCs constitute a useful tool to reduce the dynamics of the oscillator—which can be of high dimension—to a single equation for the phase. This approach, based on the phase reduction, has been extensively used to study weakly perturbed nonlinear oscillators and predict synchronization properties in neuronal networks (Canavier and Achuthan 2010; Hoppensteadt and Izhikevich 2012).

PRCs can be measured for arbitrary stimuli, both experimentally and numerically, in individual neurons and in neuronal populations, assuming that there is enough time to allow the perturbed trajectory to relax back to the limit cycle. For perturbations that are infinitesimally small in duration (pulsatile) and amplitude, one obtains the so-called infinitesimal PRC (iPRC). The iPRC corresponds to the first-order approximation of the PRC with respect to the amplitude, and it can be easily computed by solving the adjoint equation (Ermentrout and Kopell 1991). Perturbations of small amplitude but longer duration are assumed to sum linearly; thus, the phase change is obtained by convolving the input waveform with the iPRC. Of course, this approximation fails when the perturbation is strong.

Recently, there has been a large effort to compute isochrons and iPRCs accurately up to high order (Guillamon and Huguet 2009; Huguet and de la Llave 2013; Mauroy and Mezić 2012; Osinga and Moehlis 2010). Moreover, the isochrons allow for the control of the phase for trajectories away from the limit cycle. One can extend the phase coordinate system to a neighbourhood of the limit cycle by incorporating an amplitude variable. This variable is transverse to the periodic orbit and controls the “distance” to the limit cycle (Castejón et al. 2013; Wedgwood et al. 2013). This coordinate is also known as isostable (Wilson and Ermentrout 2018; Wilson and Moehlis 2016). It is therefore natural to compute the amplitude response curve (ARC) (or isostable response curve IRC) which, analogously to the PRC, provides the shift in amplitude due to a perturbation.

In this paper, we present a methodology to compute the PRC for perturbations of large amplitude and not necessarily pulsatile using the parameterization method. The underlying idea of the method is to construct a particular periodic perturbation consisting of the repetition of the transient stimulus followed by a resting period when no perturbation acts. For this periodic system, we consider its corresponding stroboscopic map and we prove that, under certain conditions, the map has an invariant curve. The core mathematical result of this paper is Theorem 3.2, which gives the existence of the invariant curve and provides the relationship between the PRC and the internal dynamics of the curve. To prove the Theorem we use the coordinate system given by the phase and the amplitude variables. In these variables, the map is contractive in the amplitude direction and one can apply the results about the existence of invariant curves in Nipp and Stoffer (1992), Nipp and Stoffer (2013). Working in the original variables, one can also use theorems on the persistence of normally hyperbolic invariant manifolds with *a posteriori* format (Bates et al. 2008, 20). That is, one formulates a functional equation for the parameterization of the invariant curve and its internal dynamics. Then, if there exists an approximate solution of this invariance equation, which satisfies some explicit nondegeneracy conditions, there is a true solution nearby. Moreover, these *a posteriori* theorems provide a numerical algorithm to compute the invariant curve and its internal dynamics based on a “quasi-Newton” method. We will implement this algorithm and compute the PRC using the result in Theorem 3.2. We also present an extension of the algorithm to compute the PRC after the breakdown of the invariant curve (possibly because it loses its normal hyperbolic properties). In this case, it is possible to write an invariance equation, which can be solved approximately using similar algorithms obtaining the PRC and the ARC.

We apply our methodology to some representative examples in the literature, namely the Morris–Lecar model and the Wilson–Cowan equations, with a sinusoidal type of stimulus. As the amplitude is increased, we detect the breakdown of the curve, which we can relate with the geometry of the isochrons. Moreover, we use the modified version of the algorithms to compute the PRC beyond the breakdown of the invariant curve. We compare the PRC computed using our methodology with the one computed using the standard approach, showing a good agreement. This accuracy is maintained for all the amplitudes, including the transition from type 0 to type 1 PRC (Glass and Mackey 1988; Glass and Winfree 1984), which occurs when the perturbation sends points of the limit cycle to the phaseless sets.

The paper is organized as follows: In Sect. 2, we set the mathematical formalism. In Sect. 3, we state the main result: Theorem 3.2. In Sect. 4, we describe the numerical algorithms based on Theorem 3.2 and present the extension for the case when the invariant curve does not exist but the PRC can still be computed. In Sect. 5, we present numerical results for some representative examples. We finish with a discussion in Sect. 6. “Appendix” contains the algorithms to compute the PRC based on the parameterization method described along the manuscript.

2 Mathematical Formalism

Let us consider a smooth system of ODEs given by

$$\dot{x} = X(x) + Ap(t; A), \quad x \in \mathbb{R}^n, \quad (1)$$

where $p(t; A)$ is a function with compact support satisfying $p(t; A) = 0$ everywhere except for $0 \leq t \leq T_{\text{pert}}$ and $\max_{t \in \mathbb{R}} |p(t; A)| = 1$. Therefore, A determines the amplitude of the perturbation.

We assume that for $A = 0$ (i.e. the unperturbed case) system (1) has a hyperbolic attracting limit cycle Γ_0 of period T

$$\Gamma_0 := \{\gamma_0(t), t \in [0, T)\},$$

being γ_0 a T -periodic solution of (1).

We will denote by $\psi_A(t; t_0, x)$ the general solution of system (1). As system (1) is autonomous for $A = 0$, we know that $\psi_0(t; t_0, x) = \phi_0(t - t_0; x)$, where $\phi_0(t; x)$ is the flow of the unperturbed system. Moreover, abusing notation, we will denote by $\phi_A(t; x) = \psi_A(t; 0, x)$.

For the unperturbed case, we can define a parameterization K_0 for Γ_0 by means of the phase variable $\theta = \frac{t}{T}$, that is,

$$K_0 : \mathbb{T} := [0, 1) \rightarrow \mathbb{R}^n, \quad (2)$$

such that $K_0(\theta) = \gamma_0(\theta T)$. Thus, the dynamics for θ satisfies

$$\dot{\theta} = 1/T, \quad \text{with solution } \Psi_0(t; \theta_0) = \theta_0 + \frac{t}{T}. \quad (3)$$

Observe that $\phi_0(t; K_0(\theta)) = K_0(\theta + \frac{t}{T}) = K_0(\Psi_0(t; \theta))$.

Consider a point x in the basin of attraction \mathcal{M} (stable manifold) of the limit cycle Γ_0 . Since Γ_0 is a normally hyperbolic invariant manifold (NHIM), by NHIM theory (see Fenichel 1971/1972; Guckenheimer 1975; Hirsch et al. 1977), there exists a unique point on the limit cycle, $K_0(\theta) \in \Gamma_0$, such that

$$d(\phi_0(t; x), \phi_0(t; K_0(\theta))) \leq Ce^{-\lambda t}, \quad \text{for } t \geq 0, \quad (4)$$

where $-\lambda < 0$ is the maximal Lyapunov exponent of Γ_0 . This property allows us to assign a phase θ to any point $x \in \mathcal{M}$. Indeed, the phase function is defined as (see Guckenheimer 1975):

$$\begin{aligned} \Theta : \mathcal{M} \subset \mathbb{R}^n &\rightarrow \mathbb{T}, \\ x &\mapsto \Theta(x) = \theta, \end{aligned} \quad (5)$$

such that Eq. (4) is satisfied. The sets of points with the same asymptotic phase are called isochrons (Winfree 1974). The sets of points where the asymptotic phase is

not defined are called phaseless sets (Guckenheimer 1975). Clearly, for an attracting normally hyperbolic invariant manifold the phaseless sets are contained in $\mathbb{R}^n \setminus \mathcal{M}$.

In this context, the PRC (see Ermentrout and Terman 2010) for the perturbation $A p(t; A)$ in (1) is defined as:

$$\text{PRC}(\theta, A) = \Theta(\phi_A(T_{\text{pert}}; K_0(\theta))) - \Theta(\phi_0(T_{\text{pert}}; K_0(\theta))), \tag{6}$$

if $\phi_A(T_{\text{pert}}; K_0(\theta)) \in \mathcal{M}$. For the rest of the manuscript, abusing notation, we will denote by \mathcal{M} a bounded neighbourhood of the periodic orbit Γ_0 such that $\bar{\mathcal{M}}$ is contained in the basin of attraction of Γ_0 .

If we denote by

$$x_{\text{pert}} := \phi_A(T_{\text{pert}}; K_0(\theta)), \quad \theta_{\text{pert}} := \Theta(x_{\text{pert}}), \tag{7}$$

from (3) and (6), we have that

$$\text{PRC}(\theta, A) = \theta_{\text{pert}} - \left(\theta + \frac{T_{\text{pert}}}{T} \right). \tag{8}$$

Moreover, since $\phi_A(T_{\text{pert}} + t; K_0(\theta)) = \phi_0(t; x_{\text{pert}})$ and using the definition of the phase function given in (5), we have that

$$\text{PRC}(\theta, A) = \Theta(\phi_A(T_{\text{pert}} + t; K_0(\theta))) - \Theta(\phi_0(T_{\text{pert}} + t; K_0(\theta))), \tag{9}$$

for all $t \geq 0$.

The usual way to compute the PRC either experimentally or numerically is the following. First, one looks for the time $t_1 \gg T_{\text{pert}}$ at which some x_i -coordinate of the perturbed trajectory $\phi_A(t; K_0(\theta))$ reaches its maximum value after the perturbation is turned off. Then, one compares time t_1 with the time t_0 which is closest to t_1 at which the unperturbed trajectory $\phi_0(t; K_0(\theta))$ reaches its maximum (see Fig. 1). Finally, the PRC is given approximately by:

$$\Delta\theta = \frac{t_1 - t_0}{T}. \tag{10}$$

This approach (that we will refer to as the *standard method*) provides a good approximation of the PRC if the time to relax back to the oscillator Γ_0 is short either because there is a strong contraction (the maximal Lyapunov exponent $-\lambda$ in (4) is sufficiently negative) or because the perturbation is weak ($A \ll 1$ in (1)). Otherwise, one should wait several periods (kT , $k \in \mathbb{N}$ sufficiently large) before computing the phase difference.

In the next sections, we present theoretical and numerical results based on the parameterization method that yield novel algorithms to compute the PRC.

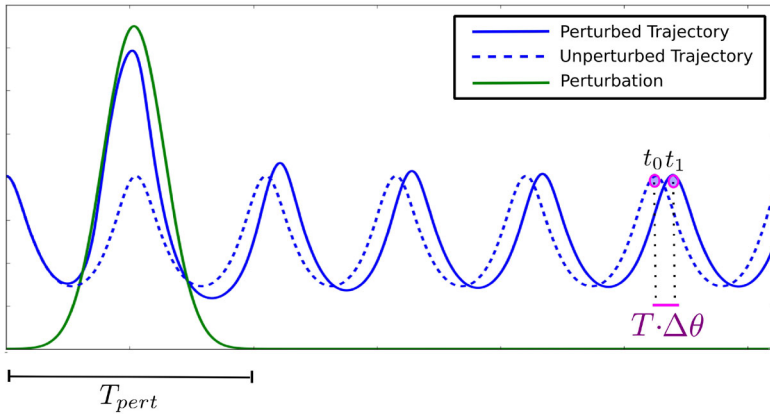


Fig. 1 After the perturbation is turned off ($t > T_{\text{pert}}$), the trajectories relax back to the limit cycle and a phase shift $\Delta\theta$ is experienced

3 Stroboscopic Approach to Compute the PRC by Means of the Parameterization Method: Theoretical Results

The perturbation $p(t; A)$ in (1) is not periodic. However, we will introduce a periodic perturbation $\bar{p}(t; A)$ of period $T' := T_{\text{pert}} + T_{\text{rel}}$, with $T_{\text{rel}} \gg T_{\text{pert}}$ which coincides with $p(t; A)$ for $0 \leq t \leq T'$. Then, we consider the T' -periodic system

$$\dot{x} = X(x) + A\bar{p}(t; A), \quad x \in \mathbb{R}^n, \tag{11}$$

whose solutions coincide with the solutions of (1) for $0 \leq t \leq T'$. Since $\bar{p}(t; A)$ is periodic, we can define the stroboscopic map given by the flow of (11) at time T' starting at $t = 0$, i.e.

$$F_A : \mathbb{R}^n \rightarrow \mathbb{R}^n, \tag{12}$$

$$x \rightarrow F_A(x) = \phi_A(T'; x) = \phi_A(T_{\text{pert}} + T_{\text{rel}}; x).$$

Using this approach, the formula for the PRC given in (9) for $t = T_{\text{rel}}$ writes as

$$\text{PRC}(\theta, A) = \Theta(F_A(K_0(\theta))) - \Theta(F_0(K_0(\theta))). \tag{13}$$

Note that for $A = 0$, one has

$$F_0(K_0(\theta)) = \phi_0(T'; K_0(\theta)) = K_0(\theta + T'/T), \tag{14}$$

and therefore

$$\Gamma_0 = \{K_0(\theta), \theta \in [0, 1)\} \tag{15}$$

is an invariant curve of the map F_0 . Moreover, by (4) we have that for any $x \in \mathcal{M}$

$$|F_0(x) - F_0(K_0(\theta))| \leq Ce^{-\lambda T'}$$

where $\theta = \Theta(x)$. Therefore, Γ_0 is a normally hyperbolic attracting invariant curve of the map F_0 .

Let us recall here, following (Fenichel 1971/1972, 1973/74; Hirsch et al. 1977), the definition of normally hyperbolic attracting invariant curve adapted to our problem.

Definition 3.1 Let $F : M \rightarrow M$ a C^r diffeomorphism on a C^r -differentiable manifold M . Assume that there exists a manifold $\Gamma \subseteq M$ that is invariant for F . We say that $\Gamma \subset M$ is a hyperbolic attracting manifold if there exists a splitting of the tangent bundle TM into DF -invariant sub-bundles, i.e.

$$TM = E^s \oplus T\Gamma,$$

and constants $C > 0$ and

$$0 < \lambda_+ < \eta^{-1} \leq 1, \tag{16}$$

such that for all $x \in \Gamma$ we have

$$\begin{aligned} v \in E_x^s &\Leftrightarrow \|DF^k(x)v\| \leq C\lambda_+^k \|v\|, \text{ for all } k \geq 0, \\ v \in T_x\Gamma &\Leftrightarrow \|DF^k(x)v\| \leq C\eta^{|k|} \|v\|, \text{ for all } k \in \mathbb{Z}. \end{aligned} \tag{17}$$

For our problem, following Guillamon and Hugué (2009); Hugué and de la Llave (2013), we can differentiate the invariance Eq. (14) of Γ_0 obtaining

$$DF_0(K_0(\theta))DK_0(\theta) = DK_0\left(\theta + \frac{T'}{T}\right), \tag{18}$$

and, for $n = 2$, in Guillamon and Hugué (2009), Hugué and de la Llave (2013) it is shown that there exists $N(\theta)$ such that

$$DF_0(K_0(\theta))N(\theta) = e^{-\lambda T'}N\left(\theta + \frac{T'}{T}\right). \tag{19}$$

Therefore, for any $x = K_0(\theta) \in \Gamma_0$, there is a splitting $\mathbb{R}^2 = \langle DK_0(\theta) \rangle \oplus \langle N(\theta) \rangle$ and rates $\lambda_+ = e^{-\lambda T'}$ and $\eta = 1$, satisfying (17) thus showing that Γ_0 is a normally hyperbolic attracting manifold. This result can be generalized to $n > 2$ using the information provided by the variational equations along the periodic orbit Γ_0 (see Remark 3.4).

Next, we present the main result of this paper which provides the existence of an invariant curve Γ_A of the stroboscopic map F_A (12) which is $\mathcal{O}(Ae^{-\lambda T_{\text{rel}}})$ -close to Γ_0 and relates its internal dynamics with the PRC of Γ_0 in system (1) (see Fig. 2). The proof of this theorem is given in Sect. 3.1.

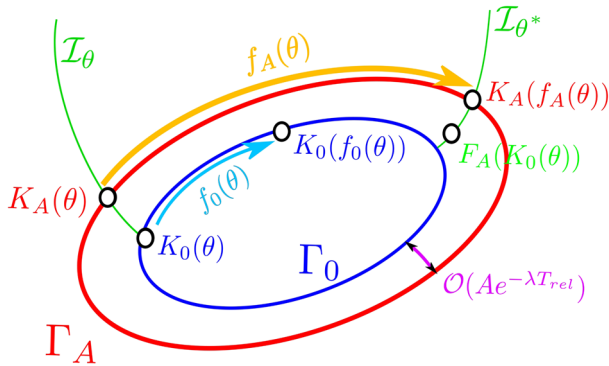


Fig. 2 Sketch of the results of Theorem 3.2. The perturbation acting on a point $K_0(\theta) \in \Gamma_0$ for a time $T' = T_{\text{pert}} + T_{\text{rel}}$ displaces it to a point $F_A(K_0(\theta))$. In Theorem 3.2, we show that the phase difference between the perturbed and unperturbed trajectories is given up to an error $\mathcal{O}(Ae^{-\lambda T_{\text{rel}}})$ by the difference between the internal dynamics $f_A(\theta)$ on Γ_A and $f_0(\theta)$ on Γ_0 . For the sake of clarity, we have located the points $K_0(\theta)$ and $K_A(\theta)$ (resp. $F_A(K_0(\theta))$ and $K_A(f_A(\theta))$) on the same isochron \mathcal{I}_θ (resp. \mathcal{I}_{θ^*} , where $\theta^* := f_A(\theta)$) although they are $\mathcal{O}(Ae^{-\lambda T_{\text{rel}}})$ -close

Theorem 3.2 Consider the stroboscopic map of the T' -periodic system (11) defined in (12) with $T' = T_{\text{pert}} + T_{\text{rel}}$ and let Γ_0 be the normally hyperbolic attracting invariant curve of the map F_0 , parameterized by K_0 , such that

$$F_0 \circ K_0 = K_0 \circ f_0,$$

where $f_0(\theta) = \theta + T'/T$.

Consider $A > 0$. Assume that A is small or $A = \mathcal{O}(1)$ and the following hypotheses are satisfied:

- H1** $\phi_A(T_{\text{pert}}; x) \in \mathcal{M}$ for any $x \in \Gamma_0$,
- H2** The function $\text{PRC}(\theta, A) + \theta$ is a monotone function,
- H3** T_{rel} is sufficiently large,

then, there exists an invariant curve Γ_A of the map F_A . Moreover, there exist a parameterization K_A of Γ_A and a periodic function f_A such that

$$\begin{aligned} F_A(K_A(\theta)) &= K_A(f_A(\theta)), \\ K_A(\theta) &= K_0(\theta) + \mathcal{O}(Ae^{-\lambda T_{\text{rel}}}), \\ \text{PRC}(\theta, A) &= f_A(\theta) - f_0(\theta) + \mathcal{O}(Ae^{-\lambda T_{\text{rel}}}). \end{aligned} \tag{20}$$

3.1 Proof of Theorem 3.2

3.1.1 The Case A Small

In this section, we prove Theorem 3.2 for A small. We first prove the following lemma which shows that the map F_A has an invariant curve Γ_A which is $\mathcal{O}(Ae^{-\lambda T_{\text{rel}}})$ -close to Γ_0 .

Lemma 3.3 *Consider the stroboscopic map of the T' -periodic system (11) defined in (12), and let Γ_0 be the normally hyperbolic invariant curve of the map F_0 , parameterized by K_0 [see (2)]. Then, for A small enough there exists an invariant curve Γ_A of the map F_A . Moreover, there exist a parameterization $K_A : \mathbb{T} \rightarrow \mathbb{R}^n$ and a periodic function $f_A : \mathbb{T} \rightarrow \mathbb{T}$ satisfying the invariance equation*

$$F_A(K_A(\theta)) = K_A(f_A(\theta)),$$

such that $K_A(\theta)$ satisfies

$$|K_A(\theta) - K_0(\theta)| = \mathcal{O}(Ae^{-\lambda T_{\text{rel}}}), \tag{21}$$

where $-\lambda < 0$ is the maximal Lyapunov exponent of Γ_0 .

Proof When $n = 2$, since, by (18) and (19), Γ_0 is a normally hyperbolic attracting invariant manifold of F_0 , the existence of the invariant curve for A small enough follows from Fenichel’s theorem (Fenichel 1971/1972, 1973/74). We will perform the rest of the proof for $n = 2$, but it can be easily generalized to arbitrary n (see Remark 3.4). Using the results in Guillamon and Hugué (2009) (see Cabré et al. 2005; Castelli et al. 2015 for higher dimensions) we can describe a point $(x, y) \in \mathcal{M}$ in terms of the so-called phase–amplitude variables. More precisely, consider the change of coordinates

$$\begin{aligned} K : \Omega \subset \mathbb{T} \times \mathbb{R} &\rightarrow \mathcal{M} \subset \mathbb{R}^2 \\ (\theta, \sigma) &\rightarrow K(\theta, \sigma) = (x, y), \end{aligned} \tag{22}$$

where $\Omega := \mathbb{T} \times U$ and $U \subset \mathbb{R}$, such that system (11) for $A = 0$, expressed in the variables (θ, σ) , has the following form

$$\begin{aligned} \dot{\theta} &= \frac{1}{T}, \\ \dot{\sigma} &= -\lambda\sigma. \end{aligned} \tag{23}$$

Moreover, system (11) for $A \neq 0$ small enough, expressed in the variables (θ, σ) , writes as the T' -periodic system

$$\begin{aligned} \dot{\theta} &= \frac{1}{T} + \mathcal{O}(A), \\ \dot{\sigma} &= -\lambda\sigma + \mathcal{O}(A), \end{aligned} \tag{24}$$

and we will denote by $\Psi_A(t; t_0, \theta, \sigma)$ the general solution of (24).

Consider now the stroboscopic map F_A in the variables (θ, σ) , i.e. $\tilde{F}_A : \Omega \rightarrow \Omega$, such that $\tilde{F}_A = K^{-1} \circ F_A \circ K$. We have

$$\tilde{F}_A(\theta, \sigma) = \Psi_A(T'; 0, \theta, \sigma) = \left(\theta_{\text{pert}} + \frac{T_{\text{rel}}}{T}, \sigma_{\text{pert}} e^{-\lambda T_{\text{rel}}} \right), \tag{25}$$

where $K(\theta_{\text{pert}}, \sigma_{\text{pert}}) = \phi_A(T_{\text{pert}}; K(\theta, \sigma)) \in \mathcal{M}$. For A small enough, we have

$$(\theta_{\text{pert}}, \sigma_{\text{pert}}) = \Psi_A(T_{\text{pert}}; 0, \theta, \sigma) = \left(\theta + \frac{T_{\text{pert}}}{T} + \mathcal{O}(A), \sigma e^{-\lambda T_{\text{pert}}} + \mathcal{O}(A) \right).$$

In conclusion,

$$\tilde{F}_A(\theta, \sigma) = \left(\theta + \frac{T'}{T} + \mathcal{O}(A), \sigma e^{-\lambda T'} + \mathcal{O}(Ae^{-\lambda T_{\text{rel}}}) \right) = \tilde{F}_0 + \mathcal{O}(A). \tag{26}$$

The unperturbed invariant curve Γ_0 in the variables (θ, σ) is given by:

$$\tilde{\Gamma}_0 = \{(\theta, \sigma) \mid \theta \in \mathbb{T}, \sigma = 0\}.$$

Therefore, by Fenichel’s theorem, for $A \neq 0$ small enough, there exists a function

$$\begin{aligned} S_A : \mathbb{T} &\rightarrow \mathbb{R} \\ \theta &\rightarrow S_A(\theta), \end{aligned} \tag{27}$$

such that $S_A(\theta) = \mathcal{O}(A)$ and the perturbed invariant curve for \tilde{F}_A is given by:

$$\tilde{\Gamma}_A = \{(\theta, \sigma) \mid \theta \in \mathbb{T}, \sigma = S_A(\theta)\}. \tag{28}$$

Analogously, $\tilde{K}_A(\theta) = (\theta, S_A(\theta))$ is a parameterization of the invariant curve $\tilde{\Gamma}_A$. Hence, using the invariance property, we have

$$\begin{aligned} \tilde{F}_A(\tilde{K}_A(\theta)) &= \tilde{F}_A(\theta, S_A(\theta)) \\ &= \left(\tilde{F}_A^1(\theta, S_A(\theta)), \tilde{F}_A^2(\theta, S_A(\theta)) \right) \\ &= \left(\tilde{F}_A^1(\theta, S_A(\theta)), S_A \left(\tilde{F}_A^1(\theta, S_A(\theta)) \right) \right) \\ &= \tilde{K}_A(\tilde{F}_A^1(\theta, S_A(\theta))) \\ &:= \tilde{K}_A(f_A(\theta)), \end{aligned}$$

where the internal dynamics is given by

$$f_A(\theta) = \tilde{F}_A^1(\theta, S_A(\theta)),$$

and \tilde{F}_A^1 and \tilde{F}_A^2 correspond to the θ and σ component of \tilde{F}_A , respectively.

Using the invariance property of $\tilde{\Gamma}_A$ and expression (26) for the stroboscopic map \tilde{F}_A , we obtain:

$$S_A \left(\theta + \frac{T'}{T} + \mathcal{O}(A) \right) = S_A(\theta)e^{-\lambda T'} + \mathcal{O}(Ae^{-\lambda T_{\text{rel}}}), \quad \forall \theta \in \mathbb{T}.$$

Therefore, since $S_A(\theta) = \mathcal{O}(A)$ and $T' = T_{\text{pert}} + T_{\text{rel}}$ we get an improved bound for $S_A(\theta)$,

$$S_A(\theta) = \mathcal{O}(Ae^{-\lambda T_{\text{rel}}}).$$

Using the change of variables $(x, y) = K(\theta, \sigma)$ given in (22), we can return to the original variables. Then, assuming $(x, y) \in \Gamma_A \subset \mathcal{M}$, if A is small enough, one has

$$(x, y) = K(\theta, \sigma) = K(\theta, S_A(\theta)) = K \circ \tilde{K}_A(\theta) =: K_A(\theta). \tag{29}$$

Thus, the invariant curve can be parameterized by K_A and

$$F_A(K_A(\theta)) = F_A \circ K \circ \tilde{K}_A(\theta) = K \circ \tilde{F}_A \circ \tilde{K}_A(\theta) = K \circ \tilde{K}_A(f_A(\theta)) = K_A(f_A(\theta)),$$

that is, the internal dynamics over the invariant curve Γ_A is the same for both parameterizations. Therefore,

$$\begin{aligned} |K_A(\theta) - K_0(\theta)| &= |K \circ \tilde{K}_A(\theta) - K \circ \tilde{K}_0(\theta)| \\ &\leq \sup_{(\theta, \sigma) \in \tilde{\Omega}} |DK(\theta, \sigma)| |\tilde{K}_A(\theta) - \tilde{K}_0(\theta)| \\ &\leq \bar{C} |S_A(\theta)| \leq CAe^{-\lambda T_{\text{rel}}}, \end{aligned} \tag{30}$$

where C is a constant independent of T_{rel} and A . □

Remark 3.4 Notice that the proof can be generalized to any $n > 2$, just considering $\sigma = (\sigma_1, \dots, \sigma_{n-1}) \in \mathbb{R}^{n-1}$ and

$$\dot{\sigma} = M\sigma,$$

where M is the real canonical form of the projection onto the stable subspace of the monodromy matrix of the first variational equation along the periodic orbit:

$$\dot{x} = DX(\gamma_0(t))x.$$

The proof can be derived analogously using that $\sigma(t) = \sigma(0)e^{Mt}$ and $|\sigma_0 e^{Mt}| < |\sigma_0|e^{-\lambda t}$, where $-\lambda < 0$ is the maximal Lyapunov exponent of Γ_0 .

End of the proof of Theorem 3.2 for A small

To finish the proof of Theorem 3.2, we need to show that the internal dynamics f_A in Γ_A is close to the PRC of Γ_0 of system (1).

Consider the parameterization K_A of the invariant curve Γ_A given in Lemma 3.3, we have

$$K_A(f_A(\theta)) = F_A(K_A(\theta)) = F_A(K_0(\theta)) + F_A(K_A(\theta)) - F_A(K_0(\theta)).$$

Assuming that $\sup_{x \in \mathcal{M}} |DF_A| \leq C$ and using that $|K_A(\theta) - K_0(\theta)| = \mathcal{O}(Ae^{-\lambda T_{\text{rel}}})$ (see Lemma 3.3), we have

$$F_A(K_0(\theta)) = K_A(f_A(\theta)) + \mathcal{O}(Ae^{-\lambda T_{\text{rel}}}). \tag{31}$$

Moreover, using the formula for the PRC given in (13), we have

$$\begin{aligned} \text{PRC}(\theta, A) &= \Theta[F_A(K_0(\theta))] - \Theta[F_0(K_0(\theta))] \\ &= \Theta[K_A(f_A(\theta)) + \mathcal{O}(Ae^{-\lambda T_{\text{rel}}})] - \Theta[K_0(f_0(\theta))] \\ &= \Theta[K_A(f_A(\theta))] - \Theta[K_0(f_0(\theta))] \\ &\quad + \Theta[K_A(f_A(\theta)) + \mathcal{O}(Ae^{-\lambda T_{\text{rel}}})] - \Theta[K_A(f_A(\theta))] \\ &= f_A(\theta) - f_0(\theta) + \Theta[K_A(f_A(\theta)) + \mathcal{O}(Ae^{-\lambda T_{\text{rel}}})] - \Theta[K_A(f_A(\theta))]. \end{aligned} \tag{32}$$

Now using that $\sup_{x \in \mathcal{M}} |\nabla\Theta| \leq C$, we have

$$\text{PRC}(\theta, A) = f_A(\theta) - f_0(\theta) + \mathcal{O}(Ae^{-\lambda T_{\text{rel}}}).$$

3.1.2 The Case $A = \mathcal{O}(1)$

To prove Theorem 3.2 for $A = \mathcal{O}(1)$, one can use the results in Bates et al. (2008), which state that if a map has an approximately invariant manifold which is approximately normally hyperbolic, then the map has a true invariant manifold nearby.

Due to the strong attracting properties of the invariant curve Γ_0 , it is straightforward to see that Γ_0 is approximately invariant for the map F_A , even if $A = \mathcal{O}(1)$.

Consider the intermediate map

$$F_{\text{pert}}(x) = \phi_A(T_{\text{pert}}; x), \tag{33}$$

we will use the hypothesis **H1** that states that F_{pert} maps the curve Γ_0 into its basin of attraction \mathcal{M} .

Then, given a point $x = K_0(\theta) \in \Gamma_0$, if $x_{\text{pert}} = F_{\text{pert}}(x) = \phi_A(T_{\text{pert}}; x) \in \mathcal{M}$, [see (7)], by Eq. (4), there exists a point $K_0(\theta_{\text{pert}}) \in \Gamma_0$ such that, for $t \geq 0$

$$\left| F_A(K_0(\theta)) - K_0\left(\theta_{\text{pert}} + \frac{T_{\text{rel}}}{T}\right) \right| = |\phi_0(T_{\text{rel}}; x_{\text{pert}}) - \phi_0(T_{\text{rel}}; K_0(\theta_{\text{pert}}))| \leq Ce^{-\lambda T_{\text{rel}}}. \tag{34}$$

Using the formula for the PRC given in (8), we have that

$$\theta_{\text{pert}} + \frac{T_{\text{rel}}}{T} = \text{PRC}(\theta, A) + \theta + \frac{T_{\text{pert}}}{T} + \frac{T_{\text{rel}}}{T} = \text{PRC}(\theta, A) + f_0(\theta), \tag{35}$$

where $f_0(\theta) = \theta + T'/T$. Hence, defining

$$\bar{f}_A(\theta) := \text{PRC}(\theta, A) + f_0(\theta), \tag{36}$$

expression (34) reads as

$$|F_A(K_0(\theta)) - K_0(\bar{f}_A(\theta))| \leq C e^{-\lambda T_{\text{rel}}}. \tag{37}$$

In other words, the curve Γ_0 with inner dynamics \bar{f}_A is approximately invariant for the map F_A with an error $\mathcal{O}(e^{-\lambda T_{\text{rel}}})$ that can be made as small as we want taking T_{rel} large enough. To apply the results in Bates et al. (2008), one needs to show that Γ_0 is approximately normally hyperbolic for F_A . That is, for each point $x \in \Gamma_0$ there exists a decomposition $\Gamma_{0,x} = \Gamma_{0,x}^c \oplus \Gamma_{0,x}^s$, with $\Gamma_{0,x}^c$ being an approximation of the tangent space to Γ_0 at x , such that

- The splitting is approximately invariant under the linearized map DF_A ,
- $DF_A(x)|_{\Gamma_0^s}$ expands and does so to a greater rate than $DF_A(x)|_{\Gamma_0^c}$ does.

Again, we will consider the two-dimensional case, but results can be generalized to arbitrary dimension (see Remark 3.4). Using the change of variables K introduced in (22) the map F_A satisfies [see Eq. (25)]:

$$F_A(K(\theta, \sigma)) = K \left(\theta_{\text{pert}} + \frac{T_{\text{rel}}}{T}, \sigma_{\text{pert}} e^{-\lambda T_{\text{rel}}} \right), \tag{38}$$

where $K(\theta_{\text{pert}}, \sigma_{\text{pert}}) = F_{\text{pert}}(K(\theta, \sigma))$ [see (33)]. Notice that θ_{pert} and σ_{pert} are correctly defined as long as $F_{\text{pert}}(K(\theta, \sigma)) \in \mathcal{M}$, which is satisfied for points $(\theta, 0)$ on the invariant curve Γ_0 by hypothesis **H1** and therefore in a small neighbourhood of Γ_0 . Taking derivatives with respect to θ and σ in expression (38), we have

$$\begin{aligned} DF_A(K(\theta, \sigma))D_\theta K(\theta, \sigma) &= D_\theta K \left(\theta_{\text{pert}} + \frac{T_{\text{rel}}}{T}, \sigma_{\text{pert}} e^{-\lambda T_{\text{rel}}} \right) \frac{\partial \theta_{\text{pert}}}{\partial \theta} \\ &\quad + D_\sigma K \left(\theta_{\text{pert}} + \frac{T_{\text{rel}}}{T}, \sigma_{\text{pert}} e^{-\lambda T_{\text{rel}}} \right) e^{-\lambda T_{\text{rel}}} \frac{\partial \sigma_{\text{pert}}}{\partial \theta}, \\ DF_A(K(\theta, \sigma))D_\sigma K(\theta, \sigma) &= D_\theta K \left(\theta_{\text{pert}} + \frac{T_{\text{rel}}}{T}, \sigma_{\text{pert}} e^{-\lambda T_{\text{rel}}} \right) \frac{\partial \theta_{\text{pert}}}{\partial \sigma} \\ &\quad + D_\sigma K \left(\theta_{\text{pert}} + \frac{T_{\text{rel}}}{T}, \sigma_{\text{pert}} e^{-\lambda T_{\text{rel}}} \right) e^{-\lambda T_{\text{rel}}} \frac{\partial \sigma_{\text{pert}}}{\partial \sigma}. \end{aligned} \tag{39}$$

Evaluating the above expression on the points $(\theta, 0)$, we have

$$\begin{aligned} DF_A(K_0(\theta))DK_0(\theta) &= D_\theta K \left(\bar{f}_A(\theta), \sigma_{\text{pert}}(\theta, 0) e^{-\lambda T_{\text{rel}}} \right) \frac{\partial \theta_{\text{pert}}}{\partial \theta}(\theta, 0) \\ &\quad + D_\sigma K \left(\bar{f}_A(\theta), \sigma_{\text{pert}}(\theta, 0) e^{-\lambda T_{\text{rel}}} \right) e^{-\lambda T_{\text{rel}}} \frac{\partial \sigma_{\text{pert}}}{\partial \theta}(\theta, 0), \\ DF_A(K_0(\theta))K_1(\theta) &= D_\theta K \left(\bar{f}_A(\theta), \sigma_{\text{pert}}(\theta, 0) e^{-\lambda T_{\text{rel}}} \right) \frac{\partial \theta_{\text{pert}}}{\partial \sigma}(\theta, 0) \\ &\quad + D_\sigma K \left(\bar{f}_A(\theta), \sigma_{\text{pert}}(\theta, 0) e^{-\lambda T_{\text{rel}}} \right) e^{-\lambda T_{\text{rel}}} \frac{\partial \sigma_{\text{pert}}}{\partial \sigma}(\theta, 0), \end{aligned} \tag{40}$$

where \bar{f}_A is defined in (36) [see also (35)] and

$$K_1(\theta) := D_\sigma K(\theta, \sigma)|_{\sigma=0}. \tag{41}$$

Now, we Taylor expand the function $K(\theta, \sigma)$ around $\sigma = 0$ and obtain

$$\begin{aligned}
 DF_A(K_0(\theta))DK_0(\theta) &= \left[DK_0(\tilde{f}_A(\theta)) + e^{-\lambda T_{\text{rel}}}\sigma_{\text{pert}}(\theta, 0)DK_1(\tilde{f}_A(\theta)) \right] \frac{\partial\theta_{\text{pert}}}{\partial\theta}(\theta, 0) \\
 &\quad + K_1(\tilde{f}_A(\theta))e^{-\lambda T_{\text{rel}}}\frac{\partial\sigma_{\text{pert}}}{\partial\theta}(\theta, 0) + \mathcal{O}(e^{-2\lambda T_{\text{rel}}}), \\
 DF_A(K_0(\theta))K_1(\theta) &= \left[DK_0(\tilde{f}_A(\theta)) + e^{-\lambda T_{\text{rel}}}\sigma_{\text{pert}}(\theta, 0)DK_1(\tilde{f}_A(\theta)) \right] \frac{\partial\theta_{\text{pert}}}{\partial\sigma}(\theta, 0) \\
 &\quad + K_1(\tilde{f}_A(\theta))e^{-\lambda T_{\text{rel}}}\frac{\partial\sigma_{\text{pert}}}{\partial\sigma}(\theta, 0) + \mathcal{O}(e^{-2\lambda T_{\text{rel}}}).
 \end{aligned}
 \tag{42}$$

Moreover, as the functions $\theta_{\text{pert}}(\theta, \sigma)$ and $\sigma_{\text{pert}}(\theta, \sigma)$ are smooth functions at the points $(\theta, 0)$, we can ensure that the error terms are uniform with respect to $\theta \in \mathbb{T}$. Let us now define

$$Z(\theta) = \frac{\partial\theta_{\text{pert}}}{\partial\sigma}(\theta, 0)DK_0(\theta) - \frac{\partial\theta_{\text{pert}}}{\partial\theta}(\theta, 0)K_1(\theta),$$

straightforward computations give

$$DF_A(K_0(\theta))Z(\theta) = \mathcal{O}(e^{-\lambda T_{\text{rel}}}).$$

Therefore, calling $\varepsilon = e^{-\lambda T_{\text{rel}}}$, we have

$$\begin{aligned}
 DF_A(K_0(\theta))DK_0(\theta) &= \Lambda_T(\theta)DK_0(\tilde{f}_A(\theta)) + \mathcal{O}(\varepsilon), \\
 DF_A(K_0(\theta))Z(\theta) &= \mathcal{O}(\varepsilon),
 \end{aligned}
 \tag{43}$$

with

$$\Lambda_T(\theta) = \frac{\partial\theta_{\text{pert}}}{\partial\theta}(\theta, 0),
 \tag{44}$$

and as long as

$$\frac{\partial\theta_{\text{pert}}}{\partial\theta}(\theta, 0) \neq 0, \theta \in \mathbb{T},
 \tag{45}$$

which is guaranteed by hypothesis **H2**, one can produce an iteration procedure to construct an approximate splitting by which Γ_0 becomes approximately normally hyperbolic (see Definition 3.1). Then, we apply the results in Bates et al. (2008), which yield that F_A will have an invariant curve Γ_A near Γ_0 .

A more direct argument consists in considering the map F_A in the variables (θ, σ) in (22), denoted by \tilde{F}_A in (25), and apply the results in Nipp and Stoffer (1992) (see also Nipp and Stoffer 2013) to this map. Thanks to hypothesis **H1**, one can consider a neighbourhood of Γ_0 where the change of variables $(x, y) = K(\theta, \sigma)$ is defined, and therefore, the map \tilde{F}_A is a smooth diffeomorphism

$$\tilde{F}_A : \mathcal{D}_\rho := \mathbb{T} \times \mathcal{I}_\rho \rightarrow \mathbb{T} \times \mathbb{R},$$

where $\mathcal{I}_\rho = \{\sigma \in \mathbb{R}, |\sigma| \leq \rho\}$, with $\rho > 0$ small, and has the form

$$\tilde{F}_A(\theta, \sigma) = \begin{pmatrix} f_0(\theta) + \hat{f}(\theta, \sigma) \\ g(\theta, \sigma) \end{pmatrix},$$

where

$$f_0(\theta) = \theta_{\text{pert}}(\theta, 0) + \frac{T_{\text{rel}}}{T}, \quad \hat{f}(\theta, \sigma) = \theta_{\text{pert}}(\theta, \sigma) - \theta_{\text{pert}}(\theta, 0), \quad g(\theta, \sigma) = \sigma_{\text{pert}}(\theta, \sigma)e^{-\lambda T_{\text{rel}}}.$$

Hypothesis **H2** ensures that f_0 is a smooth diffeomorphism (and therefore invertible). Taking T_{rel} large enough, the map \tilde{F}_A strongly contracts in the σ direction. Moreover, for $(\theta, \sigma) \in \mathcal{D}_\rho$, we have

$$\left| \frac{\partial \hat{f}}{\partial \theta} \right| \leq L_{11}, \quad \left| \frac{\partial \hat{f}}{\partial \sigma} \right| \leq L_{12}, \quad \left| \frac{\partial g}{\partial \theta} \right| \leq L_{21}, \quad \left| \frac{\partial g}{\partial \sigma} \right| \leq L_{22},$$

where $L_{11}, L_{12} = \mathcal{O}(\rho)$, $L_{21}, L_{22} = \mathcal{O}(e^{-\lambda T_{\text{rel}}})$ can be made small by taking ρ small and T_{rel} large. One can then apply Theorem 3 in Nipp and Stoffer (1992), which give, for T_{rel} large enough (hypothesis **H3**), the existence of the invariant curve in form (28), where the function S_A must satisfy

$$\tilde{F}_A^2(\theta, S_A(\theta)) = S_A(\tilde{F}_A^1(\theta, S_A(\theta))),$$

and $S_A = \mathcal{O}(e^{-\lambda T_{\text{rel}}})$. Again, \tilde{F}_A^1 and \tilde{F}_A^2 correspond to the θ and σ components of \tilde{F}_A , respectively.

Returning to the original variables $x = K(\theta, \sigma)$ defined in (22) and using that $\Gamma_A \subset \mathcal{M}$, we obtain the parameterization K_A of Γ_A as in (29). Moreover, once we have bounded the size of S_A , an analogous reasoning to (30) gives

$$|K_A(\theta) - K_0(\theta)| \leq Ce^{-T_{\text{rel}}}. \tag{46}$$

End of the Proof of Theorem 3.2 for $A = \mathcal{O}(1)$

To finish the proof of Theorem 3.2, we need to show that the internal dynamics f_A in Γ_A is close to the PRC of Γ_0 for system (1).

This can be done analogously to the case A small using (46) instead of (21) arriving to

$$\text{PRC}(\theta, A) = f_A(\theta) - f_0(\theta) + \mathcal{O}(e^{-\lambda T_{\text{rel}}}). \tag{47}$$

This step concludes the proof.

4 Computation of the PRC by Means of the Parameterization Method

Theorem 3.2 establishes that the PRC can be obtained from the dynamics f_A of the stroboscopic map F_A on the invariant curve Γ_A . This allows us to take advantage of

the existing algorithms based on the parameterization method (Cabr e et al. 2005; Haro et al. 2016) to compute the parameterization of the invariant curve K_A as well as its internal dynamics f_A . The algorithms are based on a Newton-like method to solve the invariance Eq. (20) for the unknowns K_A and f_A . Indeed, given an approximation of the parameterization of the invariant curve K_A and its internal dynamics f_A , the method provides improved solutions that solve the invariance equation up to an error which is quadratic with respect to the initial one at each step. Moreover, the method requires to compute alongside the invariant normal bundle of the invariant curve $N(\theta)$ and its linearized dynamics $\Lambda(\theta)$. In order to make the paper self-contained, the algorithms are reviewed in detail in “Appendix A”.

4.1 Computation of the PRC Beyond the Existence of the Invariant Curve

The results of Theorem 3.2 rely on the computation of an invariant curve for the stroboscopic map F_A of a system with an “artificially” constructed periodic perturbation [see Eq. (11)]. In some cases, as we will see in the numerical examples presented in Sect. 5, the invariant curve Γ_A does not exist. This situation can happen if $F_{\text{pert}}(\Gamma_0)$ is not in the basin of attraction \mathcal{M} of the limit cycle Γ_0 (breaking hypothesis **H1**), or if $\theta_{\text{pert}}(\theta, 0)$ has a critical point θ^* and therefore $d\theta_{\text{pert}}/d\theta(\theta^*, 0) = 0$ (breaking hypothesis **H2**). However, when the hypothesis **H2** fails, it is possible to design an algorithm based on the parameterization method (Canadell and Haro 2016), to compute the PRC with enough accuracy by means of solving an approximate invariance equation.

Using (38) with $\sigma = 0$, we have

$$F_A(K_0(\theta)) = K\left(\theta_{\text{pert}}(\theta, 0) + \frac{T_{\text{rel}}}{T}, \sigma_{\text{pert}}(\theta, 0)e^{-\lambda T_{\text{rel}}}\right) = K(\bar{f}_A(\theta), \bar{C}_A(\theta)),$$

where $\bar{f}_A(\theta)$ is given in (36) and

$$\bar{C}_A(\theta) := \sigma_{\text{pert}}(\theta, 0)e^{-\lambda T_{\text{rel}}}. \quad (48)$$

Taylor expanding $K(\theta, \sigma)$ with respect to σ , we obtain

$$F_A(K_0(\theta)) = K_0(\bar{f}_A(\theta)) + \mathcal{O}(e^{-\lambda T_{\text{rel}}}). \quad (49)$$

Of course, expression (49) is only valid if $F_{\text{pert}}(\Gamma_0) \in \mathcal{M}$ (hypothesis **H1**), but we do not impose that Γ_0 is approximately normally hyperbolic. Nevertheless, we will use the ideas in the algorithms reviewed in “Appendix A” and we will design a quasi-Newton method to compute a function g_A that satisfies

$$F_A(K_0(\theta)) - K_0(g_A(\theta)) = E(\theta), \quad (50)$$

where the error E cannot be smaller than the terms $\mathcal{O}(e^{-\lambda T_{\text{rel}}})$ that we have dropped.

Assuming that g_A satisfies Eq. (50), we look for an improved solution $\hat{g}_A(\theta) = g_A(\theta) + \Delta g_A(\theta)$ such that \hat{g}_A solves the approximate invariance equation up to an error which is quadratic in E . Thus, if we linearize about g_A we have

$$\begin{aligned}
 F_A(K_0(\theta)) - K_0(\hat{g}_A(\theta)) &= F_A(K_0(\theta)) - K_0(g_A(\theta)) - DK_0(g_A(\theta))\Delta g_A(\theta) + \mathcal{O}(|\Delta g_A|^2) \\
 &= E(\theta) - DK_0(g_A(\theta))\Delta g_A(\theta) + \mathcal{O}(|\Delta g_A|^2).
 \end{aligned}
 \tag{51}$$

Therefore, we look for Δg_A satisfying the equation

$$E(\theta) = DK_0(g_A(\theta))\Delta g_A(\theta),$$

which provides

$$\Delta g_A(\theta) = \frac{\langle DK_0(g_A(\theta)), E(\theta) \rangle}{\langle DK_0(g_A(\theta)), DK_0(g_A(\theta)) \rangle}, \tag{52}$$

where $\langle \cdot, \cdot \rangle$ denotes the dot product.

Remark 4.1 Notice that expression (52) corresponds to the projection of E onto the tangent direction DK_0 , thus obtaining Δg_A in the same way as Δf_A in Algorithm A.2 (see ‘‘Appendix A’’).

The algorithm to compute the PRC is then:

Algorithm 4.2 Computation of the PRC. *Given a parameterization of the limit cycle $K_0(\theta)$ and an approximate solution of Eq. (50) $g_A(\theta)$, perform the following operations:*

1. Compute $E(\theta) = F_A(K_0(\theta)) - K_0(g_A(\theta))$.
2. Compute $DK_0(g_A(\theta))$.
3. Compute $\Delta g_A = \frac{\langle DK_0(g_A(\theta)), E(\theta) \rangle}{\langle DK_0(g_A(\theta)), DK_0(g_A(\theta)) \rangle}$.
4. Set $g_A(\theta) \leftarrow g_A(\theta) + \Delta g_A(\theta)$.
5. Repeat steps 1–4 until the error E is smaller than the established tolerance. Then $\text{PRC}(\theta, A) = g_A(\theta) - (\theta + T'/T)$.

In Sect. 5, we apply Algorithm 4.2 to several examples, illustrating the convergence of the method and the good agreement of the results with the standard method.

4.2 Computation of the PRC and ARC

In the previous section, we have used that K_0 satisfies Eq. (49). Notice that we can be more precise and include the exact expression of the terms of $\mathcal{O}(e^{-\lambda T_{\text{rel}}})$, that is,

$$F_A(K_0(\theta)) = K_0(\bar{f}_A(\theta)) + K_1(\bar{f}_A(\theta))\bar{C}_A(\theta) + \mathcal{O}(e^{-2\lambda T_{\text{rel}}}),$$

with $K_1(\theta)$ as in (41).

We already know that the function $\bar{f}_A(\theta)$ provides the PRC through relation (36). We would like to emphasize here the role of $\bar{C}_A(\theta)$ defined in (48). The analogous curve to the PRC for the amplitude σ is known as the amplitude response curve (Castej3n et al. 2013; Wilson and Moehlis 2015) (ARC) and is given by $\text{ARC}(\theta) = \sigma_{\text{pert}}(\theta, 0)$,

that is, the value of σ at x_{pert} [see (7)]. Therefore, since $\sigma_{\text{pert}}(\theta, 0) = \bar{C}_A(\theta)e^{\lambda T_{\text{rel}}}$, the function $\bar{C}_A(\theta)$ provides the ARC through the expression $ARC(\theta, A) = \bar{C}_A(\theta)e^{\lambda T_{\text{rel}}}$.

As in the previous section, it is possible to design a quasi-Newton method to compute the functions g_A and C_A that satisfy

$$F_A(K_0(\theta)) - K_0(g_A(\theta)) - C_A(\theta)K_1(g_A(\theta)) = E(\theta), \tag{53}$$

where the error E will not be smaller than the terms of order $\mathcal{O}(e^{-2\lambda T_{\text{rel}}})$ that we have dropped.

Proceeding as in the previous section, we assume that g_A and C_A satisfy Eq. (53) and we look for improved solutions, $\hat{g}_A(\theta) = g_A(\theta) + \Delta g_A(\theta)$ and $\hat{C}_A(\theta) = C_A(\theta) + \Delta C_A(\theta)$, such that \hat{g}_A and \hat{C}_A solve the approximate invariance equation up to an error which is quadratic in E . Thus, if we linearize about g_A and C_A , we have

$$\begin{aligned} &F_A(K_0(\theta)) - K_0(\hat{g}_A(\theta)) - K_1(\hat{g}_A(\theta))\hat{C}_A(\theta) \\ &= F_A(K_0(\theta)) - K_0(g_A(\theta)) - DK_0(g_A(\theta))\Delta g_A(\theta) - K_1(g_A(\theta))C_A(\theta) \\ &\quad - DK_1(g_A(\theta))\Delta g_A(\theta)C_A(\theta) - K_1(g_A(\theta))\Delta C_A(\theta) + \mathcal{O}(\Delta^2, e^{-2\lambda T_{\text{rel}}}) \\ &= E(\theta) - DK_0(g_A(\theta))\Delta g_A(\theta) - DK_1(g_A(\theta))\Delta g_A(\theta)C_A(\theta) \\ &\quad - K_1(g_A(\theta))\Delta C_A(\theta) + \mathcal{O}(\Delta^2). \end{aligned} \tag{54}$$

Hence, we are left with the following equation for Δg_A and ΔC_A ,

$$E(\theta) = [DK_0(g_A(\theta)) + DK_1(g_A(\theta))C_A(\theta)]\Delta g_A(\theta) + K_1(g_A(\theta))\Delta C_A(\theta). \tag{55}$$

Therefore, the unknown Δg_A corresponds to the projection of the error E onto the direction $R := DK_0 \circ g_A + C_A \cdot DK_1 \circ g_A$ and $\Delta C_A(\theta)$ corresponds to the projection of E onto the K_1 direction. Of course, DK_0 and K_1 are transversal since K_1 is tangent to the isochrons of the unperturbed limit cycle, which are always transversal to the limit cycle. Since $C_A = \mathcal{O}(e^{-\lambda T_{\text{rel}}})$, assuming that T_{rel} is large enough, we can always guarantee that R and K_1 are transversal. Therefore, multiplying (55) by $K_1^\perp(g_A(\theta))$, we have

$$\Delta g_A(\theta) = \frac{\langle K_1^\perp(g_A(\theta)), E(\theta) \rangle}{\langle K_1^\perp(g_A(\theta)), R(\theta) \rangle}, \tag{56}$$

whereas multiplying by $R(\theta)^\perp$, we obtain

$$\Delta C_A(\theta) = \frac{\langle R^\perp(\theta), E(\theta) \rangle}{\langle R^\perp(\theta), K_1(g_A(\theta)) \rangle}, \tag{57}$$

where $\langle \cdot, \cdot \rangle$ denotes the dot product.

Remark 4.3 Notice that $C_A(\theta) = \mathcal{O}(e^{-\lambda T_{\text{rel}}})$, and if we disregard the terms $\mathcal{O}(e^{-\lambda T_{\text{rel}}})$ in expression (56), we obtain

$$\Delta g_A(\theta) = \frac{\langle K_1^\perp(g_A(\theta)), E(\theta) \rangle}{\langle K_1^\perp(g_A(\theta)), DK_0(g_A(\theta)) \rangle}, \tag{58}$$

which is equivalent to the expression obtained in (52). Indeed, in this case the vectors $E(\theta)$ and $DK_0(\theta)$ have the same direction, and expression (52) can be replaced by

$$\Delta g_A(\theta) = \frac{\langle v, E(\theta) \rangle}{\langle v, DK_0(g_A(\theta)) \rangle},$$

where v can be any vector as long as it is not perpendicular to $DK_0(g_A(\theta))$.

Thus, the algorithm to compute the PRC and the ARC is:

Algorithm 4.4 Computation of the PRC and the ARC. *Given a parameterization of the limit cycle $K_0(\theta)$, the tangent vector to the isochrons of the limit cycle $K_1(\theta)$, and approximate solutions of Eq. (53) $g_A(\theta)$ and $C_A(\theta)$, perform the following operations:*

1. Compute $E(\theta) = F_A(K_0(\theta)) - K_0(g_A(\theta)) - C_A(\theta)K_1(g_A(\theta))$.
2. Compute $R(\theta) = DK_0(g_A(\theta)) + DK_1(g_A(\theta))C_A(\theta)$.
3. Compute $\Delta g_A(\theta) = \frac{\langle K_1^\perp(g_A(\theta)), E(\theta) \rangle}{\langle K_1^\perp(g_A(\theta)), R(\theta) \rangle}$.
4. Compute $\Delta C_A(\theta) = \frac{\langle R^\perp(\theta), E(\theta) \rangle}{\langle R^\perp(\theta), K_1(g_A(\theta)) \rangle}$.
5. Set $g_A(\theta) \leftarrow g_A(\theta) + \Delta g_A(\theta)$.
6. Set $C_A(\theta) \leftarrow C_A(\theta) + \Delta C_A(\theta)$.
7. Repeat steps 1–6 until the error E is smaller than the established tolerance. Then,

$$\text{PRC}(\theta, A) = g_A(\theta) - (\theta + T'/T),$$

and

$$\text{ARC}(\theta, A) = C_A(\theta)e^{\lambda T_{\text{rel}}}.$$

5 Numerical Examples

In this section, we apply the algorithms based on the parameterization method introduced in Sect. 4 to compute the PRC to some relevant models in neuroscience, namely the Wilson–Cowan model (Wilson and Cowan 1972) and the Morris–Lecar model (Morris and Lecar 1981). We will use the same perturbation for both models:

$$p(t) = \sin^6\left(\frac{\pi t}{T_{\text{pert}}}\right),$$

for $0 \leq t \leq T_{\text{pert}}$ and $T_{\text{pert}} = 10$. The value of T_{rel} is different for each model, and its value is indicated with the other parameters of the model in Tables 1 and 2, respectively.

In order to validate the algorithms, we will compare the results obtained using the parameterization method with the *standard method* (see formula (10)).

The Wilson–Cowan model The Wilson–Cowan model describes the behaviour of a coupled network of excitatory and inhibitory neurons. The perturbed model has the form (see Wilson and Cowan 1972):

$$\begin{aligned}\dot{E} &= -E + S_e(aE - bI + P + Ap(t)), \\ \dot{I} &= -I + S_i(cE - dI + Q),\end{aligned}\quad (59)$$

where the variables E and I are the firing rate activity of the excitatory and inhibitory populations, respectively, and

$$S_k(x) = \frac{1}{1 + e^{-a_k(x - \theta_k)}}, \quad \text{for } k = e, i, \quad (60)$$

is the response function.

We consider two sets of parameters, for which the system displays a limit cycle. For the first set of parameters the limit cycle is born from a Hopf bifurcation, and for the second one from a saddle node on invariant circle (SNIC) bifurcation (Borisjuk and Kirillov 1992). We refer to them as WC-Hopf and WC-SNIC, respectively. Some parameters of the model are common to both cases, namely $a = 13$, $b = 12$, $c = 6$, $d = 3$, $a_e = 1.3$, $a_i = 2$, $\theta_e = 4$, $\theta_i = 1.5$. Parameters (P, Q) for each set are given in Table 1, together with the period T , the characteristic exponent $-\lambda$ of each periodic orbit, and the relaxation time T_{rel} of the perturbation.

We compute the PRC for the limit cycle of the Wilson–Cowan model for different values of the amplitude A . In Figs. 3 and 4, we show the comparison between the PRCs computed using the standard method and the parameterization method for the WC-Hopf and the WC-SNIC, respectively. We remark the good agreement between both methods.

We also show the invariant curve Γ_A , the internal dynamics f_A and the derivative of f_A in Fig. 5 for the WC-Hopf and in Fig. 6 for the WC-SNIC. Notice that as A increases, the shape of the PRC shows a sudden increase for certain phase values (see panel A in Figs. 5 and 6). A more detailed discussion about this phenomenon will be given in Sect. 5.1.

The Morris–Lecar model It was originally developed to study the excitability properties for the muscle fibre of the giant barnacle, and it has been established as a paradigm for the study of different neuronal excitability types (Rinzel and Ermentrout 1989; Rinzel and Huguet 2013). The perturbed model has the form (see Morris and Lecar 1981):

$$\begin{aligned}C\dot{V} &= I_{\text{app}} - g_L(V - V_L) - g_K w(V - V_K) - g_{\text{Ca}} m_\infty(V)(V - V_{\text{Ca}}) + Ap(t), \\ \dot{w} &= \phi \frac{w_\infty(V) - w}{\tau_w(V)},\end{aligned}\quad (61)$$

Table 1 (P, Q) parameter values for the Wilson–Cowan model close to the corresponding type of bifurcation

Parameter	Hopf	SNIC
P	2.5	1.45
Q	0	-0.75
T	5.26	13.62
T_{rel}	15T	6T
$-\lambda$	-0.157	-0.66

For the indicated parameter values and $A = 0$, system (59) has a stable limit cycle of period T and characteristic exponent $-\lambda$

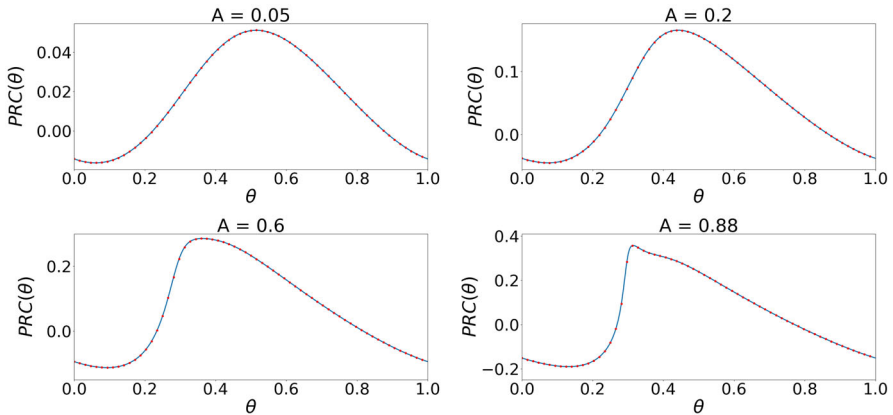


Fig. 3 PRCs for the Wilson–Cowan model near a Hopf bifurcation (WC-Hopf) for different values of the amplitude A (as indicated in each panel) showing the comparison between the parameterization method (solid blue line) and the *standard method* (red dots) (Color figure online)

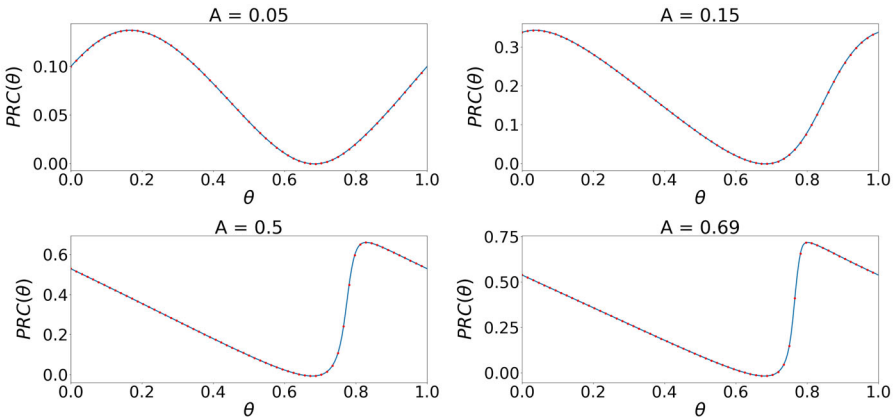


Fig. 4 PRCs for the Wilson–Cowan near a SNIC bifurcation (WC-SNIC) for different values of the amplitude A (as indicated in each panel) showing the comparison between the parameterization method (solid blue line) and the *standard method* (red dots) (Color figure online)

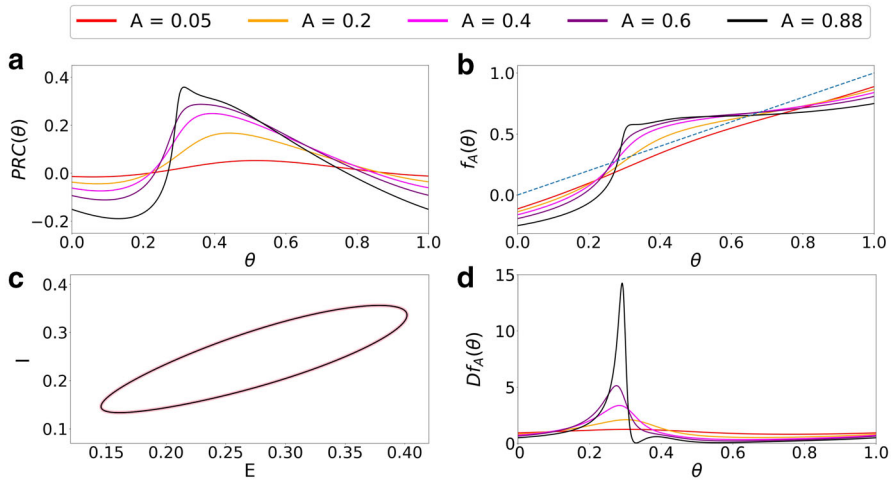


Fig. 5 For the Wilson–Cowan model near a Hopf bifurcation (WC-Hopf) and different amplitude values A we show: **a** the PRCs, **b** the dynamics $f_A(\theta)$ on the invariant curve Γ_A , **c** the invariant curve Γ_A , **d** the derivative of $f_A(\theta)$. The dashed blue line in panel **b** corresponds to the identity function (Color figure online)

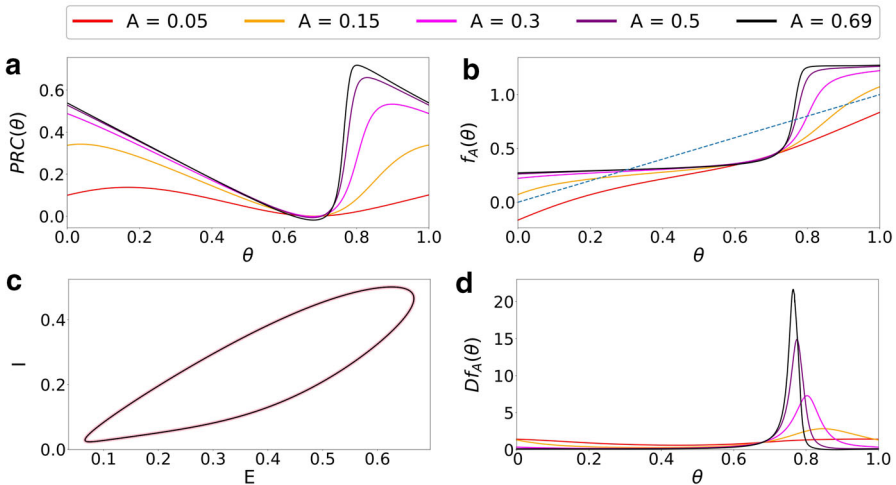


Fig. 6 For the Wilson–Cowan model near a SNIC bifurcation (WC-SNIC) and different amplitude values A we show: **a** the PRCs, **b** the dynamics $f_A(\theta)$ on the invariant curve Γ_A , **c** the invariant curve Γ_A , **d** the derivative of $f_A(\theta)$. The dashed blue line in panel **b** corresponds to the identity function (Color figure online)

where

$$\begin{aligned}
 m_\infty(V) &= \frac{1}{2}(1 + \tanh((V - V_1)/V_2)), \\
 w_\infty(V) &= \frac{1}{2}(1 + \tanh((V - V_3)/V_4)), \\
 \tau_w(V) &= (\cosh((V - V_3)/(2V_4)))^{-1}.
 \end{aligned}
 \tag{62}$$

Table 2 Parameter values for the Morris–Lecar model close to the corresponding type of bifurcation

Parameter	Hopf	SNIC
ϕ	0.04	0.067
g_{Ca}	4.4	4
V_3	2	12
V_4	30	17.4
I_{app}	91	45
T	99.27	99.192
T_{rel}	6T	5T
$-\lambda$	-0.0919	-0.1198

For the indicated parameter values and $A = 0$, system (61) has a stable periodic orbit of period T and characteristic exponent $-\lambda$.

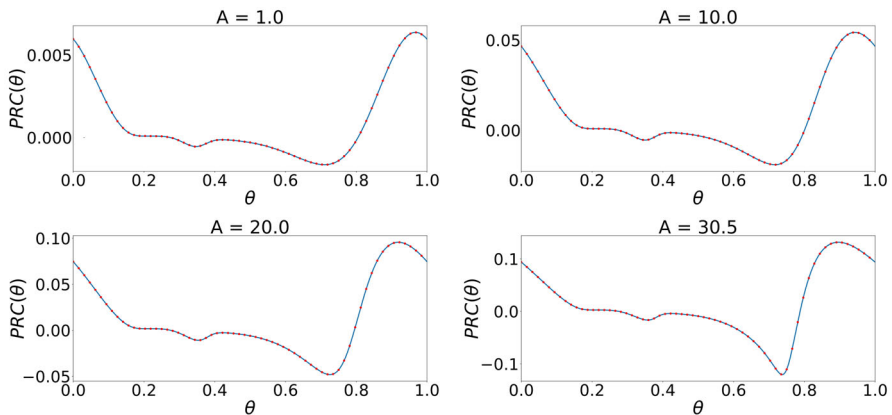


Fig. 7 PRCs for the Morris–Lecar model near a Hopf bifurcation (ML-Hopf) for different values of the amplitude (indicated in each panel) showing the comparison between the parameterization method (solid blue line) and the *standard method* (red dots) (Color figure online)

As in the previous example, we consider two sets of parameters for which the system displays a limit cycle across a Hopf and a SNIC bifurcation (Ermentrout and Terman 2010; Rinzel and Huguet 2013). We will refer to them as MC-Hopf and MC-SNIC, respectively. Some parameters of the model will be common to both cases, namely $C = 20$, $V_L = -60$, $V_K = -84$, $V_{Ca} = 120$, $V_1 = -1.2$, $V_2 = 18$, $g_L = 2$, $g_K = 8$. The other parameter values are listed in Table 2.

We compute the PRC for different values of the amplitude A . In Figs. 7 and 8, we show the comparison between the standard method and the parameterization method for ML-Hopf and ML-SNIC, respectively. Again, we remark the good agreement between both methods. Other elements of the computation of the PRCs using the parameterization method are shown in Figs. 9 and 10. Again, both cases show a sharp rise in the PRC for certain phase values as the amplitude increases. We refer the reader to Sect. 5.1 for a more detailed discussion.

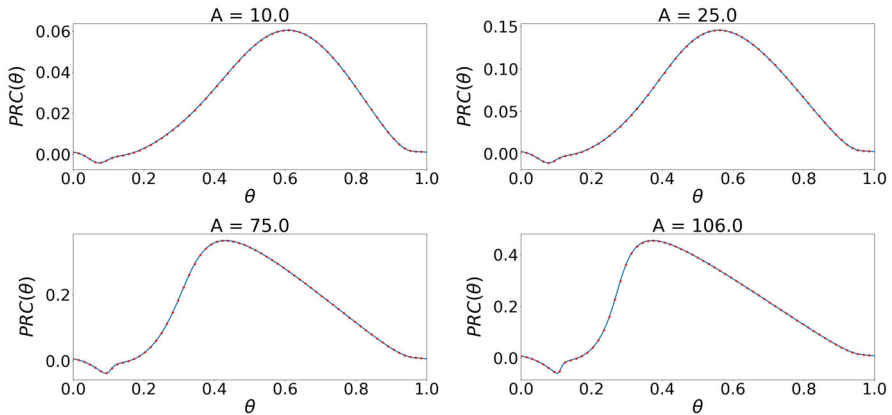


Fig. 8 PRCs for the Morris–Lecar model near a SNIC bifurcation (ML-SNIC) for different values of the amplitude (indicated in each panel) showing the comparison between the parameterization method (solid blue line) and the *standard method* (red dots) (Color figure online)

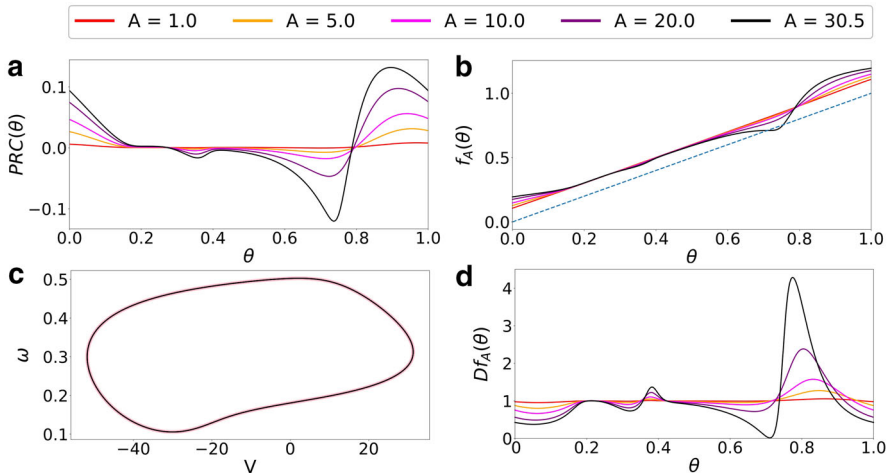


Fig. 9 For the Morris–Lecar near a Hopf bifurcation (ML-Hopf) and different amplitude values we show: **a** the PRCs, **b** the dynamics $f_A(\theta)$ on the invariant curve Γ_A , **c** the invariant curve Γ_A , **d** the derivative of $f_A(\theta)$. The dashed blue line in panel **b** corresponds to the identity function

5.1 Large Amplitude Perturbations

The application of the parameterization method using the algorithms in “Appendix A” (see Sect. 4) strongly relies on the existence of an invariant curve Γ_A for the stroboscopic map of a system with an “artificially” constructed periodic perturbation (see Theorem 3.2). In the numerical examples shown in Figs. 5, 6, 9 and 10, the computation of the invariant curve fails when the amplitude becomes large and approaches a certain value A^* (which is different for each example), and so does the computation of the PRC using this method. In this section, we will discuss how changes in the wave-

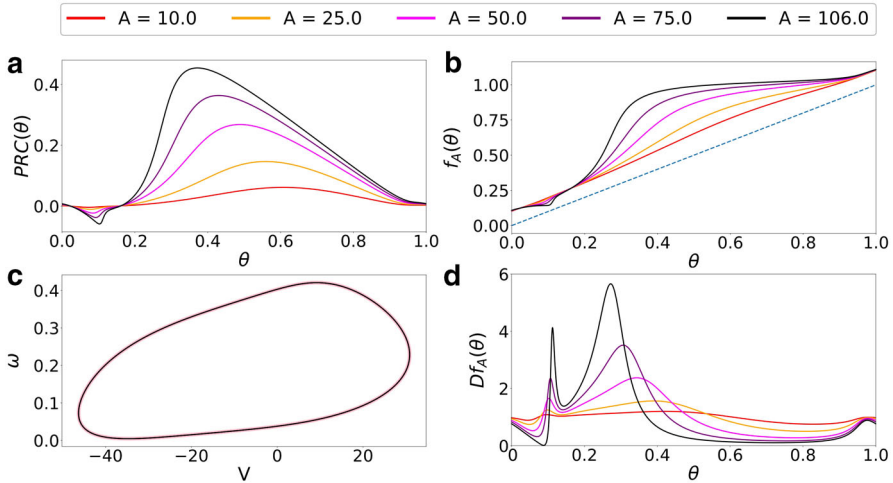


Fig. 10 For the Morris–Lecar near a SNIC bifurcation (ML-SNIC) and different amplitude values we show: **a** the PRCs, **b** the dynamics $f_A(\theta)$ on the invariant curve Γ_A , the invariant curve Γ_A , **d** the derivative of $f_A(\theta)$. The dashed blue line in panel **b** corresponds to the identity function

form of the PRC might be related to normally hyperbolic properties of the invariant curve. We will first focus our discussion on the WC-Hopf model.

First notice that, as the amplitude A increases, the PRC becomes steeper (see Fig. 5a). By looking at the internal dynamics f_A on the invariant curve Γ_A (see Fig. 5b), we observe that as the amplitude increases, the curve f_A shows a sharp rise followed by a flat region. Moreover, there appear stable and unstable fixed points on the invariant curve Γ_A (intersection of f_A with the identity line in Fig. 5b). Thus, the curve Γ_A preserves its normal hyperbolicity as long as the contraction/expansion rates on the invariant curve are weaker than the contraction rates on the normal directions [see Eq. (43)]. Indeed, since the contraction rate in the normal direction is $\mathcal{O}(e^{-\lambda T_{rel}})$ [see (43)], this means that $Df_A(\theta) = d\theta_{pert}/d\theta$ must remain bounded away from 0 [see (45)]. However, we observe that as A increases the value of Df_A approaches 0 for a certain θ (see Fig. 5d), thus causing the loss of the normal hyperbolicity property and the breakdown of the curve. For values of A slightly smaller than the one for which $Df_A(\theta)$ vanishes, the numerical method in “Appendix A” fails to converge. However, we can apply the modified parameterization method provided by the algorithms in Sect. 4 and compute the function g_A [see Eq. (50)] and the PRC beyond the existence of an invariant curve (see Fig. 11b–d right).

Notice that the method in Algorithm 4.2 also works if the invariant curve exists (see Fig. 11a right). In this case, g_A is $\mathcal{O}(e^{-\lambda T_{rel}})$ -close to f_A [see Eqs. (36), (47), (49), (53)]. Therefore, for practical purposes, the modified method is faster and accurate enough to compute the PRC.

It is possible to describe the phenomenon of the breakdown of the curve in a geometric way using the concept of isochrons (curves of constant phase) and phaseless sets of the original limit cycle. For the model considered, the isochrons for the unperturbed limit cycle are shown in Fig. 11 (left). Notice that the unperturbed system has

an unstable focus P for which the isochrons are not defined (the phaseless set). Now, we consider the image of the curve Γ_0 under the map F_{pert} introduced in (33), for different values of A . Of course, the intersection of the curve $\Gamma_{\text{pert}} = F_{\text{pert}}(\Gamma_0)$ with the isochrons provides the new phases. For small values of A , Γ_{pert} will intersect all the isochrons transversally leading to every possible new phase in a one-to-one correspondence (see Fig. 11a). Accordingly, the functions $f_A(\theta)$ and $g_A(\theta)$ are diffeomorphisms.

However, as A increases, there exists a value A^* for which the curve Γ_{pert} becomes tangent to some isochrons, and therefore, the curve Γ_{pert} intersects some isochrons more than once (see Fig. 11b). Thus, the map g_A is no longer one-to-one, which means that Dg_A vanishes for certain phases, causing the loss of normal hyperbolicity and the breakdown of the curve.

Clearly, the function g_A for $A = 0.95$ shows a local maximum and minimum (see Fig. 11b right), corresponding to an isochron tangency. When A is increased further, the function g_A splits into two. Indeed, the curve Γ_{pert} will first intersect the phaseless point P for a certain value $A \approx 1.035$ (see Fig. 11c) and after that it will no longer enclose the point P , so it will not cross all the isochrons of the limit cycle (see Fig. 11d). The map g_A will then be discontinuous at the point where the curve Γ_{pert} intersects the phaseless set. After that, the function g_A will be continuous again when we take modulus 1, but, of course, the images will not span the whole interval $[0, 1)$. Regarding the winding number classification for PRCs, defined as the number of times the curve Γ_{pert} traverses a complete cycle as defined by the isochrons of the unperturbed limit cycle (Glass and Mackey 1988; Glass and Winfree 1984), for $A \approx 1.035$ there is a transition from a type 1 PRC to a type 0 PRC.

The modified parameterization method introduced in Sect. 4.2 allows for the computation of the amplitude response curve (ARC) (see Algorithm 4.4). The ARCs for the amplitude values considered in Fig. 11 are shown in Fig. 12. The ARC provides information about how “far” in time the perturbation displaces the trajectory away from the limit cycle. That is, the larger the value of the ARC, the longer it will take for the displaced trajectory to relax back to the limit cycle (and therefore one should consider a larger T_{rel}).

Notice that when the curve Γ_{pert} intersects the phaseless set (point P), which occurs for a critical amplitude $A_c \approx 1.035$, there exists a perturbed trajectory which never returns to the limit cycle, and the ARC would show an essential discontinuity. Thus, for smaller values of the amplitude $A < A_c$, the ARC shows a peak whose size increases as the amplitude A is increased towards A_c (see Fig. 12a–c). However, for amplitude values larger than A_c (Fig. 12d), the ARC peak decreases again with A , because Γ_{pert} moves away from the neighbourhood of the phaseless point P .

A similar phenomenon as discussed for the WC-Hopf occurs for the WC-SNIC and ML-SNIC examples. The Morris–Lecar model near a Hopf bifurcation (ML-Hopf) is slightly different, since in this case the phaseless set is larger compared to the WC-Hopf case: it is a positive measure set bounded by an unstable limit cycle Γ_u which determines the basin of attraction of the equilibrium point lying in its interior (see Fig. 13a). As in the WC-Hopf case, the invariant curve Γ_A for the ML-Hopf disappears due to an isochron tangency of Γ_{pert} . Consistently with this tangency, Γ_{pert} for $A = 33$ crosses some isochrons more than once (see Fig. 13a and zoom in b) and

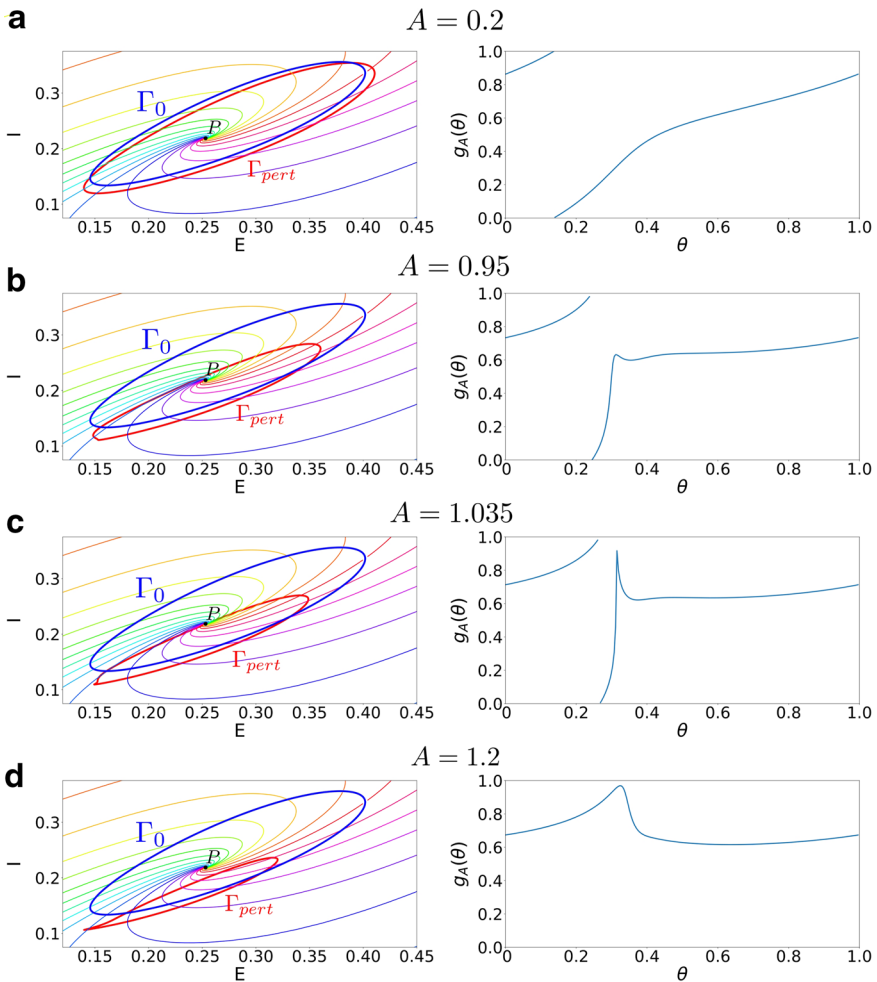


Fig. 11 For different values of the amplitude (indicated in each panel), we show the isochrons of the unperturbed limit cycle Γ_0 for the Wilson–Cowan model near a Hopf bifurcation (WC-Hopf), together with the curves Γ_{pert} (left) and the functions g_A obtained with the modified parameterization method (right). The amplitudes selected cover the breakdown of the curve Γ_A and a transition from type 1 to type 0 PRCs (see text)

as Fig. 13c, d shows, the function g_A loses its monotonicity. Nevertheless, one can still compute the PRC by means of Algorithm 4.2. By contrast, for larger amplitude values, several points of Γ_{pert} leave the basin of attraction of the stable limit cycle (see Fig. 13a and zoom in b for $A = 40$). Thus, the PRC can no longer be computed even with the modified method.

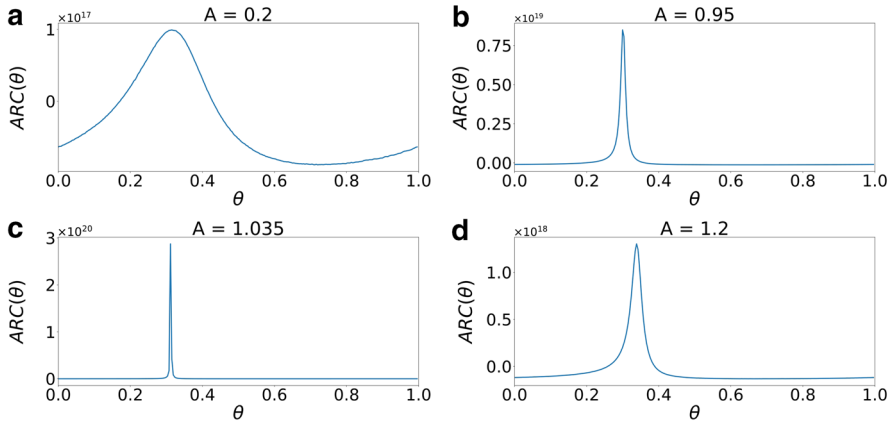


Fig. 12 ARCs for the Wilson–Cowan model near a Hopf bifurcation (WC-Hopf) and different values of the amplitude (same as in Fig. 11)

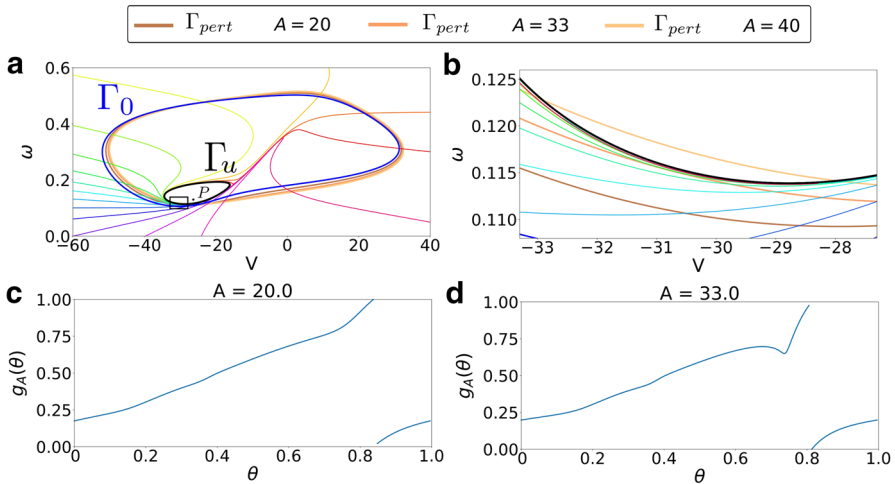


Fig. 13 Phase space for the ML-Hopf showing the stable limit cycle Γ_0 , its isochrons, and the unstable limit cycle Γ_u determining the basin of attraction of a stable focus P . For different values of the amplitude, we show (a) the curves Γ_{pert} and (b) a zoom close to the isochron tangency. Panels (c) and (d) show the functions g_A obtained with the modified parameterization method for $A = 20$ (c) and $A = 33$ (d). For $A = 40$ some points on Γ_{pert} intersect the basin of attraction of the stable focus P , and the function g_A cannot be computed

6 Discussion

In this paper, we have introduced a new approach to PRCs based on the parameterization method. The main idea of the method is to introduce a periodic perturbation consisting of the actual perturbation followed by a relaxation time T_{rel} that repeats periodically. This periodic perturbation allows us to define the corresponding stroboscopic map F_A of the periodically perturbed system. The main result of this paper is

Theorem 3.2, where we prove the existence of an invariant curve Γ_A for the map F_A and we link its internal dynamics f_A with the PRC. The proof relies on the parameterization method, which defines an invariance equation for the invariant curve and its internal dynamics (Cabr e et al. 2005; Canadell and Haro 2014; Haro and de la Llave 2006, 2007), and provides a numerical algorithm to compute both.

Moreover, Theorem 3.2 establishes conditions for the existence of the invariant curve Γ_A . More precisely, although the range of amplitude values A for which the invariant curve exists can be increased by considering a sufficiently large T_{rel} , there is a limitation established by the geometry of the isochrons. Indeed, whenever the curve Γ_{pert} (the displacement of the limit cycle due to the active part of the perturbation) becomes tangent to some isochron of Γ_0 , the invariant curve Γ_A loses its normally hyperbolic properties and breaks down. Moreover, we explain how the isochrons of the unperturbed system and the perturbation interact to shape the waveform of the PRC as the amplitude of the perturbation increases.

Besides theoretical results, we present some strategies to compute the PRC. In Haro et al. (2016), one can find algorithms that implement a quasi-Newton method to solve the above-mentioned invariance equation. The method though relies on the existence of an invariant curve. Nevertheless, as the PRC can be computed beyond the breakdown of the curve Γ_A , we have developed a modified numerical method to compute PRCs inspired by the parameterization method. This method solves a modified invariance equation, which avoids the computation of the invariant curve (thus making the computations faster) and is able to compute PRCs beyond the breakdown of the curve Γ_A and the transition from type 1 to type 0 PRCs. In addition, this algorithm computes not only PRCs but also ARCs, which provide information about the effects of the perturbation onto the amplitude variables (or alternatively, the displacement away from the limit cycle). We show examples of the computed ARCs and the relationship between its shape and the transitions experienced by the PRC.

In order to assess the validity of the method, we have applied it to two models in neuroscience: a neural population model (Wilson–Cowan) and a single neuron model (Morris–Lecar). Moreover, we have studied both models for values of the parameters near two different bifurcations: Hopf and saddle node on invariant circle (SNIC) bifurcations. Recall that PRCs are classified as types 1 or 2 according to their shape, and this property is associated with a particular bifurcation: type 1 PRCs mainly advance phase, and they are related to a SNIC bifurcation, while type 2 PRCs can either advance or delay the phase, and they are related to a Hopf bifurcation (Ermentrout 1996; Oprisan and Canavier 2002; Smeal et al. 2010). The numerical examples presented show the evolution of both PRC types for large amplitude values. In all the examples considered, the PRCs preserve its type as the amplitude increases, but the phase shifts tend to augment.

In this work, we have mainly developed the theory and numerical examples for two-dimensional systems. However, the underlying theorems and numerical algorithms have an straightforward extension for the case $n > 2$ that we plan to explore in detail in future work.

Acknowledgements This work has been partially funded by the Grants MINECO-FEDER MTM2015-65715-P, MDM-2014-0445, PGC2018-098676-B-100 AEI/FEDER/UE, the Catalan Grant 2017SGR1049,

(GH, AP, TS), the MINECO-FEDER-UE MTM-2015-71509-C2-2-R (GH), and the Russian Scientific Foundation Grant 14-41-00044 (TS). GH acknowledges the RyC project RYC-2014-15866. TS is supported by the Catalan Institution for research and advanced studies via an ICREA academia price 2018. AP acknowledges the FPI Grant from project MINECO-FEDER-UE MTM2012-31714. We thank C. Bonet for providing us valuable references to prove Theorem 3.2 and A. Granados for numeric support. We also acknowledge the use of the UPC Dynamical Systems group's cluster for research computing (<https://dynamicalsystems.upc.edu/en/computing/>).

A Appendix: Numerical Algorithms

In this section, we review the numerical algorithms introduced in Haro et al. (2016) to compute the parameterization of an invariant curve Γ_A of a given map $F := F_A$ as well as the dynamics on the curve, i.e. $f := F|_{\Gamma_A}$. We present the algorithms in a format that is ready for numerical implementation, and we refer the reader to Haro et al. (2016), Pérez-Cervera et al. (2018) for more details.

The method to compute the invariant curve consists in looking for a map $K : \mathbb{T} \rightarrow \mathbb{R}^2$ and a scalar function $f : \mathbb{T} \rightarrow \mathbb{T}$ satisfying the invariance equation

$$F(K(\theta)) = K(f(\theta)). \quad (63)$$

In order to solve Eq. (63) by means of a Newton-like method, one needs to compute alongside the invariant normal bundle of K , denoted by N , and its linearized dynamics Λ_N , which satisfy the invariance equation

$$DF(K(\theta))N(\theta) = DK(f(\theta))\Lambda_N(\theta). \quad (64)$$

Thus, the main algorithm provides a Newton method to solve Eqs. (63) and (64) altogether. More precisely, at step i of the Newton method one computes successive approximations K^i, f^i, N^i and Λ_N^i of K, f, N and Λ_N , respectively. The algorithm is stated as follows:

Algorithm A.1 Main Algorithm to Solve Equations (63), (64). Given $K(\theta), f(\theta), f^{-1}(\theta), N(\theta)$ and $\Lambda_N(\theta)$, approximate solutions of Eqs. (63) and (64), perform the following operations:

1. Compute the corrections $\Delta K(\theta)$ and $\Delta f(\theta)$ by using Algorithm A.2.
2. Update $K(\theta) \leftarrow K(\theta) + \Delta K(\theta)$ $f(\theta) \leftarrow f(\theta) + \Delta f(\theta)$.
3. Compute the inverse function $f^{-1}(\theta)$ using Algorithm A.3.
4. Compute $DK(\theta)$ and $Df(\theta)$.
5. Compute the corrections $\Delta N(\theta)$ and $\Delta \Lambda_N(\theta)$ by using Algorithm A.5.
6. Update $N(\theta) \leftarrow N(\theta) + \Delta N(\theta)$ $\Lambda_N(\theta) \leftarrow \Lambda_N(\theta) + \Delta \Lambda_N(\theta)$.
7. Compute $E = F \circ K - K \circ f$ and repeat steps 1–6 until E is smaller than the established tolerance.

Next, we provide the sub-algorithms for Algorithm A.1.

Algorithm A.2 Correction of the Approximate Invariant Curve. Given $K(\theta), f(\theta), f^{-1}(\theta), N(\theta)$ and $\Lambda_N(\theta)$, approximate solutions of Eqs. (63) and (64), perform the following operations:

1. Compute $E(\theta) = F(K(\theta)) - K(f(\theta))$.
2. Compute $P(f(\theta)) = \left(DK(f(\theta)) | N(f(\theta)) \right)$.
3. Compute $\eta(\theta) = \begin{pmatrix} \eta_T(\theta) \\ \eta_N(\theta) \end{pmatrix} = -(P(f(\theta)))^{-1} E(\theta)$.
4. Compute $f^{-1}(\theta)$ using Algorithm A.3.
5. Solve for ξ the equation $\eta_N(f^{-1}(\theta)) = \Lambda_N(f^{-1}(\theta))\xi(f^{-1}(\theta)) - \xi(\theta)$ by using Algorithm A.4.
6. Set $\Delta f(\theta) \leftarrow -\eta_T(\theta)$.
7. Set $\Delta K(\theta) \leftarrow N(\theta)\xi(\theta)$.

Algorithm A.3 Refine $f^{-1}(\theta)$. Given a function $f(\theta)$, its derivative $Df(\theta)$ and an approximate inverse function $f^{-1}(\theta)$, perform the following operations:

1. Compute $e(\theta) = f(f^{-1}(\theta)) - \theta$.
2. Compute $\Delta f^{-1}(\theta) = -\frac{e(\theta)}{Df(f^{-1}(\theta))}$.
3. Set $f^{-1}(\theta) \leftarrow f^{-1}(\theta) + \Delta f^{-1}(\theta)$.
4. Repeat steps 1–3 until $e(\theta)$ is smaller than a fixed tolerance.

Algorithm A.4 Solution of a fixed point equation. Given an equation of the form $B(\theta) = A(\theta)\eta(g(\theta)) - \eta(\theta)$ with A, B, g known and $\|A\| < 1$, perform the following operations:

1. Set $\eta(\theta) \leftarrow B(\theta)$.
2. Compute $\eta(g(\theta))$.
3. Set $\eta(\theta) \leftarrow A(\theta)\eta(g(\theta)) + \eta(\theta)$.
4. Repeat steps 2 and 3 until $|A(\theta)\eta(g(\theta))|$ is smaller than the established tolerance.

Algorithm A.5 Correction of the stable normal bundle. Given $K(\theta), f(\theta), N(\theta)$ and $\Lambda_N(\theta)$, approximate solutions of Eqs. (63) and (64), perform the following operations:

1. Compute $E_N(\theta) = DF(K(\theta))N(\theta) - \Lambda_N(\theta)N(f(\theta))$.
2. Compute $P(f(\theta)) = (DK(f(\theta)) | N(f(\theta)))$.
3. Compute $\zeta(\theta) = \begin{pmatrix} \zeta_T(\theta) \\ \zeta_N(\theta) \end{pmatrix} = -(P(f(\theta)))^{-1} E_N(\theta)$.
4. Solve for Q the equation $Df^{-1}(\theta)\zeta_T(\theta) = Df^{-1}(\theta)\Lambda_N(\theta)Q(f(\theta)) - Q(\theta)$ by using Algorithm A.4.
5. Set $\Delta_N(\theta) \leftarrow \zeta_N(\theta)$.
6. Set $\Delta N(\theta) \leftarrow DK(\theta)Q(\theta)$.

Remark A.6 Since our functions are defined on \mathbb{T} , we will use Fourier series to compute the derivatives and composition of functions.

Of course, the main algorithm requires the knowledge of an approximate solution for Eqs. (63), (64). In our case, we can always use the limit cycle of the unperturbed system as an approximate solution for the invariant curve. However, for the normal bundle we cannot use the one obtained from the unperturbed limit cycle Γ_0 . The following algorithm provides an initial seed for Algorithm A.1.

Algorithm A.7 Computation of Initial Seeds. Given a planar vector field $\dot{x} = X(x)$, having an attracting limit cycle $\gamma(t)$ of period T , perform the following operations:

1. Compute the fundamental matrix $\Phi(t)$ of the first variational equation along the periodic orbit.
2. Obtain the characteristic multiplier $\lambda \neq 1$ and its associated eigenvector v_λ from $\Phi(T)$.
3. Set $N(\theta) \leftarrow \Phi(T\theta)v_\lambda e^{\lambda\theta}$.
4. Set $\Lambda_N(\theta) \leftarrow e^{\frac{\lambda T'}{T}}$.
5. Set $K(\theta) \leftarrow \gamma(T\theta)$, $DK(\theta) = TX(\gamma(T\theta))$.
6. Set $f(\theta) \leftarrow \theta + \frac{T'}{T}$, $f^{-1}(\theta) \leftarrow \theta - \frac{T'}{T}$, $Df(\theta) = 1$.

Given a family of maps F_A such that the solution for F_0 is known (see Algorithm A.7), it is standard to set a continuation scheme to compute the solutions for the other values of A . Thus, assuming that the solution for $A = A^*$ is known, one can take this solution as an initial seed to solve the equations for F_{A^*+h} , with h small, using the Newton-like method described in Algorithm A.1. However, one can perform an extra step to refine the initial seed values K_{A^*} and f_{A^*} for F_{A^*+h} , described in Algorithm A.8.

Algorithm A.8 Refine an Initial Seed. Given $K_A(\theta)$, $f_A(\theta)$, $N_A(\theta)$ and $\Lambda_{N,A}(\theta)$, solutions of Eqs. (63), (64) for $F = F_A$, perform the following operations:

1. Compute $E(\theta) = \frac{\partial F_A}{\partial A}(K_A(\theta))$.
2. Compute $\eta(\theta) = \begin{pmatrix} \eta_T(\theta) \\ \eta_N(\theta) \end{pmatrix} = -(P(f_A(\theta)))^{-1}E(\theta)$.
3. Solve for ξ the equation $\xi(\theta) = \Lambda_N(f_A^{-1}(\theta))\xi(f_A^{-1}(\theta)) - \eta_N(f_A^{-1}(\theta))$ by using Algorithm A.4.
4. Set $K_{A+h}(\theta) \leftarrow K_A(\theta) + N_A(\theta)\xi(\theta) \cdot h$, $f_{A+h}(\theta) \leftarrow f_A(\theta) - \eta_T(\theta) \cdot h$.

Remark A.9 The term $\frac{\partial F}{\partial A}(K_A(\theta))$ is computed using variational equations with respect to the amplitude.

The numerical continuation scheme for our problem is described in the following algorithm.

Algorithm A.10 Numerical Continuation. Consider a family of maps F_A , such that F_0 is the time- T map of a planar autonomous system having a hyperbolic attracting limit cycle of period T . Perform the following operations:

1. Compute solutions $K_0(\theta)$, $f_0(\theta)$, $N_0(\theta)$ and $\Lambda_{N,0}(\theta)$ of Eqs. (63), (64) for $F = F_0$ using Algorithm A.7.
2. Set $A = 0$.
3. Using K_A , f_A , N_A , $\Lambda_{N,A}$ compute an initial seed for F_{A+h} using Algorithm A.8
4. Find solutions of Eqs. (63), (64) for $F = F_{A+h}$ using Algorithm A.1.
5. Set $A \leftarrow A + h$.
6. Repeat steps 3–5 until A reaches the desired value.

References

- Bates, P.W., Lu, K., Zeng, C.: Approximately invariant manifolds and global dynamics of spike states. *Invent. Math.* **174**(2), 355–433 (2008)
- Borisjuk, R.M., Kirillov, A.B.: Bifurcation analysis of a neural network model. *Biol. Cybern.* **66**(4), 319–325 (1992)
- Buzsáki, G.: *Rhythms of the Brain*. Oxford University Press, Oxford (2006)
- Cabré, X., Fontich, E., De La Llave, R.: The parameterization method for invariant manifolds III: overview and applications. *J. Differ. Equ.* **218**(2), 444–515 (2005)
- Canadell, M., Haro, A.: Parameterization method for computing quasi-periodic reducible normally hyperbolic invariant tori. In: *Advances in Differential Equations and Applications*, pp. 85–94. Springer, Berlin (2014)
- Canadell, M., Haro, À.: A newton-like method for computing normally hyperbolic invariant tori. In: *The Parameterization Method for Invariant Manifolds*, pp. 187–238. Springer, Berlin (2016)
- Canavier, C.C., Achuthan, S.: Pulse coupled oscillators and the phase resetting curve. *Math. Biosci.* **226**(2), 77–96 (2010)
- Castejón, O., Guillamon, A., Huguet, G.: Phase-amplitude response functions for transient-state stimuli. *J. Math. Neurosci.* **3**(1), 13 (2013)
- Castelli, R., Lessard, J.-P., Mireles James, J.D.: Parameterization of invariant manifolds for periodic orbits I: efficient numerics via the floquet normal form. *SIAM J. Appl. Dyn. Syst.* **14**(1), 132–167 (2015)
- Ermentrout, B.: Type I membranes, phase resetting curves, and synchrony. *Neural Comput.* **8**(5), 979–1001 (1996)
- Ermentrout, B., Terman, D.: *Mathematical Foundations of Neuroscience*. Springer, New York (2010)
- Ermentrout, G.B., Kopell, N.: Multiple pulse interactions and averaging in systems of coupled neural oscillators. *J. Math. Biol.* **29**(3), 195–217 (1991)
- Fenichel, N.: Persistence and smoothness of invariant manifolds for flows. *Indiana Univ. Math. J.*, **21**, 193–226, (1971/1972)
- Fenichel, N.: Asymptotic stability with rate conditions. *Indiana Univ. Math. J.*, **23**, 1109–1137 (1973/74)
- Glass, L., Mackey, M.C.: *From Clocks to Chaos: The Rhythms of Life*. Princeton University Press, Princeton (1988)
- Glass, L., Winfree, A.T.: Discontinuities in phase-resetting experiments. *Am. J. Physiol. Regul. Integr. Comp. Physiol.* **246**(2), R251–R258 (1984)
- Guckenheimer, J.: Isochrons and phaseless sets. *J. Math. Biol.* **1**(3), 259–273 (1975)
- Guillamon, A., Huguet, G.: A computational and geometric approach to phase resetting curves and surfaces. *SIAM J. Appl. Dyn. Syst.* **8**(3), 1005–1042 (2009)
- Haro, À., Canadell, M., Figueras, J.-L., Luque, A., Mondelo, J.-M.: *The Parameterization Method for Invariant Manifolds*. Springer, Berlin (2016)
- Haro, A., de la Llave, R.: Persistence of normally hyperbolic invariant manifolds, internal communication
- Haro, A., de la Llave, R.: A parameterization method for the computation of invariant tori and their whiskers in quasi-periodic maps: numerical algorithms. *Discret. Contin. Dyn. Syst. Ser. B* **6**(6), 1261 (2006)
- Haro, A., de La Llave, R.: A parameterization method for the computation of invariant tori and their whiskers in quasi-periodic maps: explorations and mechanisms for the breakdown of hyperbolicity. *SIAM J. Appl. Dyn. Syst.* **6**(1), 142 (2007)
- Hirsch, M., Pugh, C., Shub, M.: *Invariant Manifolds*. Volume 538 of *Lecture Notes in Math*. Springer, Berlin (1977)
- Hoppensteadt, F.C., Izhikevich, E.M.: *Weakly Connected Neural Networks*, vol. 126. Springer Science & Business Media, Berlin (2012)
- Huguet, G., de la Llave, R.: Computation of limit cycles and their isochrons: fast algorithms and their convergence. *SIAM J. Appl. Dyn. Syst.* **12**(4), 1763–1802 (2013)
- Mauroy, A., Mezić, I.: On the use of fourier averages to compute the global isochrons of (quasi) periodic dynamics. *Chaos Interdiscip. J. Nonlinear Sci.* **22**(3), 033112 (2012)
- Morris, C., Lecar, H.: Voltage oscillations in the barnacle giant muscle fiber. *Biophys. J.* **35**(1), 193–213 (1981)
- Nipp, K., Stoffer, D.: Attractive invariant manifolds for maps: existence, smoothness and continuous dependence on the map. In: *Research report/Seminar für Angewandte Mathematik*, volume 1992. Eidgenössische Technische Hochschule, Seminar für Angewandte Mathematik (1992)

- Nipp, K., Stoffer, D.: Invariant manifolds in discrete and continuous dynamical systems. EMS Tracts in Mathematics 21 (2013)
- Oprisan, S.A., Canavier, C.C.: The influence of limit cycle topology on the phase resetting curve. *Neural Comput.* **14**(5), 1027–1057 (2002)
- Osinga, H.M., Moehlis, J.: Continuation-based computation of global isochrons. *SIAM J. Appl. Dyn. Syst.* **9**(4), 1201–1228 (2010)
- Pérez-Cervera, A., Hugué, G., Seara, T.: *Computation of Invariant Curves in the Analysis of Periodically Forced Neural Oscillators*. Springer, Berlin (2018)
- Rinzel, J., Ermentrout, G.B.: *Analysis of Neural Excitability and Oscillations*. MIT Press, Cambridge, MA (1989)
- Rinzel, J., Hugué, G.: Nonlinear dynamics of neuronal excitability, oscillations, and coincidence detection. *Commun. Pure Appl. Math.* **66**(9), 1464–1494 (2013)
- Schultheiss, N.W., Prinz, A.A., Butera, R.J.: *Phase Response Curves in Neuroscience: Theory, Experiment, and Analysis*. Springer Science & Business Media, Berlin (2011)
- Smeal, R.M., Ermentrout, G.B., White, J.A.: Phase-response curves and synchronized neural networks. *Philos. Trans. R. Soc. Lond. B Biol. Sci.* **365**(1551), 2407–2422 (2010)
- Wedgwood, K.C., Lin, K.K., Thul, R., Coombes, S.: Phase-amplitude descriptions of neural oscillator models. *J. Math. Neurosci.* **3**(1), 2 (2013)
- Wilson, D., Ermentrout, B.: Greater accuracy and broadened applicability of phase reduction using isostable coordinates. *J. Math. Biol.* **76**(1–2), 37–66 (2018)
- Wilson, D., Moehlis, J.: Extending phase reduction to excitable media: theory and applications. *SIAM Rev.* **57**(2), 201–222 (2015)
- Wilson, D., Moehlis, J.: Isostable reduction of periodic orbits. *Phys. Rev. E* **94**(5), 052213 (2016)
- Wilson, H.R., Cowan, J.D.: Excitatory and inhibitory interactions in localized populations of model neurons. *Biophys. J.* **12**(1), 1–24 (1972)
- Winfree, A.: Patterns of phase compromise in biological cycles. *J. Math. Biol.* **1**(1), 73–93 (1974)

Publisher's Note Springer Nature remains neutral with regard to jurisdictional claims in published maps and institutional affiliations.